Identification of immune-related genes and development of a prognostic model in mantle cell lymphoma

Wei Zhang[1#], Jin-Ning Shi[1#], Hai-Ning Wang[2], Ting Zhang[1], Xuan Zhou[1], Hong-Mei Zhang[3], Feng Zhu[3]

[1]Department of Hematology, The Affiliated Jiangning Hospital of Nanjing Medical University, Nanjing, China; [2]Department of Blood Supply, Nanjing Red Cross Blood Center, Nanjing, China; [3]Department of Blood Transfusion, The Affiliated Jiangning Hospital of Nanjing Medical University, Nanjing, China

Contributions: (I) Conception and design: W Zhang, HM Zhang, F Zhu; (II) Administrative support: F Zhu, JN Shi, HM Zhang; (III) Provision of study methods: W Zhang, X Zhou, HM Zhang; (IV) Collection and assembly of data: W Zhang, HN Wang, X Zhou, T Zhang; (V) Data analysis and interpretation: W Zhang, HN Wang, T Zhang, X Zhou; (VI) Manuscript writing: All authors; (VII) Final approval of manuscript: All authors.

[#]These authors contributed equally to this work.

Correspondence to: Feng Zhu; Hong-Mei Zhang. Department of Blood Transfusion, The Affiliated Jiangning Hospital of Nanjing Medical University, Nanjing 211100, China. Email: zhm.0619@163.com; zhm.0619@126.com.

Background: The immune landscape, prognostic model, and molecular variations of mantle cell lymphoma (MCL) remain unclear. Hence, an integrated bioinformatics analysis of MCL datasets is required for the development of immunotherapy and the optimization of targeted therapies.

Methods: Data were obtained from the Gene Expression Omnibus (GEO) database (GSE32018, GSE45717 and GSE93291). The differentially expressed immune-related genes were selected, and the hub genes were screened by three machine learning algorithms, followed by enrichment and correlation analyses. Next, MCL molecular clusters based on the hub genes were identified by K-Means clustering, the probably approximately correct (PAC) algorithm, and principal component analysis (PCA). The landscape of immune cell infiltration and immune checkpoint molecules in distinct clusters was explored by single-sample gene-set enrichment analysis (ssGSEA) as well as the CIBERSORT and xCell algorithms. The prognostic genes and prognostic risk score model for MCL clusters were identified by least absolute shrinkage and selection operator (LASSO)-Cox analysis and cross-validation for lambda. Correlation analysis was performed to explore the correlation between the screened prognostic genes and immune cells or immune checkpoint molecules.

Results: Four immune-related hub genes (*CD247*, *CD3E*, *CD4*, and *GATA3*) were screened in MCL, mainly enriched in the T-cell receptor signaling pathway. Based on the hub genes, two MCL molecular clusters were recognized. The cluster 2 group had a significantly worse overall survival (OS), with down-regulated hub genes, and a variety of activated immune effector cells declined. The majority of immune checkpoint molecules had also decreased. An efficient prognostic model was established, including six prognostic genes (*LGALS2*, *LAMP3*, *ICOS*, *FCAMR*, *IGFBP4*, and *C1QA*) differentially expressed between two MCL clusters. Patients with a higher risk score in the prognostic model had a poor prognosis. Furthermore, most types of immune cells and a range of immune checkpoint molecules were positively correlated with the prognostic genes.

Conclusions: Our study identified distinct molecular clusters based on the immune-related hub genes, and showed that the prognostic model affected the prognosis of MCL patients. These hub genes, modulated immune cells, and immune checkpoint molecules might be involved in oncogenesis and could be potential prognostic biomarkers in MCL.

Keywords: Mantle cell lymphoma (MCL); immune-related genes; prognosis; bioinformatics integration analysis

Submitted Nov 02, 2022. Accepted for publication Dec 08, 2022.

doi: 10.21037/atm-22-5815

View this article at: https://dx.doi.org/10.21037/atm-22-5815

Introduction

Mantle cell lymphoma (MCL), a heterogeneous and invariably aggressive non-Hodgkin lymphoma (NHL), accounts for 5–7% of all lymphomas, with approximately 70% of cases occurring in men and a median patient age of about 60–70 years (1). MCL possesses both indolent and aggressive NHL characteristics, with a median overall survival (OS) of about 3–5 years (2), and inevitably relapses following standard frontline therapies, such as immunochemotherapy and autologous stem cell transplantation (3). Although innovative agents have improved the therapeutic options for MCL patients, the identification of individual risk profiles based on MCL complex biology and the choice of combined targeted therapies remains challenging. Therefore, further understanding of the molecular genetic background and relative prognostic factors of MCL may aid in optimizing treatments and exploring new therapeutic targets.

A series of genetic variations have been reported to participate in the pathogenesis and prognostic prediction of MCL patients. Cyclin D1 overexpression, derived from the t(11;14)(q13;q32) translocation, is the known characteristic change and is accompanied by cell cycle deregulation (4). Several prognostic biomarkers have been identified in MCL: 6 genes (*AKT3*, *BCL2*, *BTK*, *CD79B*, *PIK3CD*, and *SYK*) mostly from the B-cell receptor pathway (5); hub genes, including *KIF11*, *CDC20*, *CCNB1*, *CCNA2*, and *PUF60* (6); and 10 genes (*KIF18A*, *YBX3*, *PEMT*, *GCNA*, *POGLUT3*, *SELENOP*, *AMOTL2*, *IGFBP7*, *KCTD12*, and *ADGRG2*) related to the cell cycle, apoptosis, and metabolism (7). Based on genomic and transcriptomic profiling, four MCL molecular subsets were identified, which affected clinical outcomes and were involved in clonal evolution (8). However, the complex molecular mechanisms in MCL pathogenesis remain largely unexplored.

Cancer immunotherapy has been an effective anti-cancer treatment in recent years, and among them, the groundbreaking immune checkpoint blockade (ICB) therapies have improved the outcomes of patients with different tumors, including classical Hodgkin lymphoma and natural killer (NK)/T-cell lymphoma (9-11). Nevertheless, in the majority of hematological malignancies, the clinical benefit from ICB therapies remains limited, even when used in combination therapy (9,12). In MCL, the effects of various immune checkpoint inhibitors (ICIs) are inconclusive, and the expressions of programmed death 1 (PD-1) and its ligands are almost undetectable (13,14). Moreover, the immune-response genes and stromal microenvironments have confirmed the major roles in the survival, progression, and chemoresistance of MCL (15-17). Therefore, understanding the immune landscape and molecular variations in MCL is essential for the development of immunotherapy. Dufva *et al*. defined the multifaceted immune landscape of various hematological malignancies by integrating the data of genetic and epigenetic aberrations and the tumor microenvironment (TME) (12). A clinical immune-related prognostic model, including the predictors of B symptoms, platelet count, beta-2-microglobulin (β2-MG) level, cluster of differentiation 4 $(CD4)^+$ T-cell count <26.7%, and $CD8^+$ T-cell count >44.2%, could predict the OS of MCL patients (18). However, the immune-related hub genes, prognostic model, and underlying mechanisms of MCL require further elucidation.

In this study, we performed an integrated bioinformatics analysis of MCL datasets from the Gene Expression Omnibus (GEO) database to investigate the immune-related genes, immune infiltrated cells, and immune checkpoint molecules and identify MCL molecular clusters based on the immune-related hub genes. We also established a prognostic risk score model and explored the potential immune cell regulation and relative molecular mechanisms. The flowchart of this study is shown in *Figure 1*. We present the following article in accordance with the TRIPOD reporting checklist (available at https://atm.

Highlight box

Key findings

- The distinct molecular clusters based on immune-related hub genes were identified, and a prognostic model was established in MCL.

What is known and what is new?

- Innovative agents have improved the therapeutic options for MCL patients, however, the immune checkpoint blockade therapies remain limited.
- This study identified the immune-related hub genes and a prognostic model of MCL, and preliminary explored the potential immune cell regulation and relative molecular mechanisms.

What is the implication, and what should change now?

- The immune-related hub genes, modulated immune cells, and immune checkpoint molecules might be involved in oncogenesis and could be potential prognostic biomarkers in MCL. Further research should be carried out to examine the regulatory mechanisms and explore the efficiency of the prognostic model, for enhancing the effect of immunotherapy.

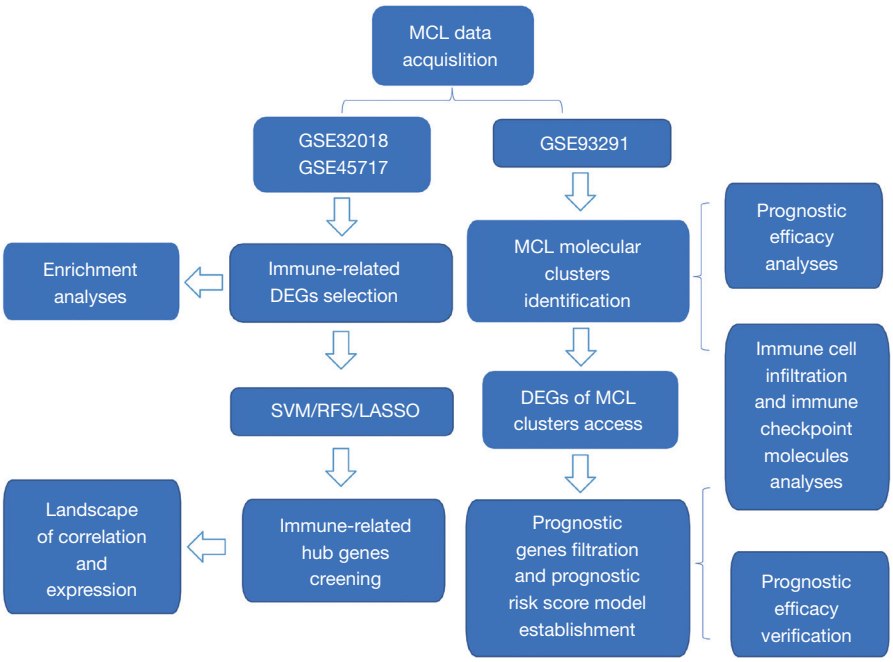

Figure 1 Study flowchart. MCL, mantle cell lymphoma; DEGs, differentially expressed genes; SVM, SVM-RFE, support vector machine-recursive feature elimination; RFS, Random forest; LASSO, least absolute shrinkage and selection operator.

amegroups.com/article/view/10.21037/atm-22-5815/rc).

Methods

Data selection and acquisition

The study was conducted in accordance with the Declaration of Helsinki (as revised in 2013). The data in this study was respectively obtained from GSE32018 (19), GSE45717 (20), and GSE93291 (21) datasets in the GEO database (http://www.ncbi.nlm.nih.gov/geo). There were 24 tumor samples and seven normal controls in GSE32018, five tumor samples and eight normal controls in GSE45717, and 123 tumor samples in GSE93291.

Expression and enrichment analyses of immune-related genes in MCL

The immune-related genes were obtained and downloaded from the GeneCards database (http://www.genecards.org/), using a keyword search of the term "immune". Using the "limma (v3.42.2)" in R software package (https://www.r-project.org/), the differentially expressed genes (DEGs) were selected between MCL tumor samples and normal controls in the GSE32018 and GSE45717 datasets. The threshold was defined as follows: adjusted P value <0.05 and |log fold change (FC)| >0.585. The common DEGs were selected and visualized via "Venn Diagram (v1.7.3)" in R package. For the Gene Ontology (GO) and Kyoto Encyclopedia of Genes and Genomes (KEGG) enrichment analyses, functional and pathway enrichment analyses of the common DEGs were performed using "clusterProfiler (v4.0)" in R package, using P<0.05 and q<0.2 as the threshold.

Screening of immune-related hub genes in MCL

The hub DEGs in MCL, which could distinguish cancerous from normal tissue, were screened in the much larger GSE32018 dataset, using three machine learning algorithms, respectively. Firstly, the hub genes were acquired using the support vector machine-recursive feature elimination (SVM-RFE) algorithm (https://github.com/johncolby/SVM-RFE) via 10-fold cross-validation.

Secondly, the hub genes were obtained by a random forest algorithm using the "RandomForest (v4.6-14)" R package, using ntree =50, and MeanDecreaseGini >0 as the threshold. Thirdly, the hub genes were selected through the least absolute shrinkage and selection operator (LASSO) algorithm using "glmnet (v4.0-2)" R package via 10-fold cross-validation for lambda. Finally, the common hub

genes from three algorithms were demonstrated by the "Venn Diagram (v1.7.3)" R package. The String database (https://cn.string-db.org/) was employed for protein-protein interaction (PPI) network analysis and functional enrichment analysis of these hub genes. The correlation among these genes was determined via Pearson's correlation analysis.

The location information of the screened immune-related hub genes was displayed in a circos ideogram using "RCircos (v1.2.1)" R package. In the GSE32018 database, the correlation between these genes was demonstrated by Pearson's correlation analysis, and scatter plots were utilized to display the gene pairs, using |correlation| >0.6. The expression of these genes between the cancer and normal samples was presented via a heatmap and scatter plot.

Identification of MCL molecular clusters based on the immune-related hub genes

The expression matrix of immune-related hub genes in the GSE93291 dataset was analyzed by K-Means clustering using the "ConsensusClusterPlus (v1.50.0)" R package. The molecular clusters of MCL were recognized via the probably approximately correct (PAC) algorithm, and Kaplan-Meier survival analysis was performed. Principal component analysis (PCA) was conducted using "factoextra (v1.0.7)" and "FactoMineR (v2.4)" R packages. The expression of these hub genes in distinct molecular clusters was displayed in a boxplot and heatmap.

The landscape of immune cell infiltration and immune checkpoint molecules in distinct MCL molecular clusters based on the immune-related hub genes

The distinct MCL molecular clusters based on the immune-related hub genes in the GSE93291 dataset was analyzed using hallmark gene sets in the Molecular Signature Database (MSigDB) (https://www.gsea-msigdb.org/gsea/msigdb/, MSigDB v7.5.1) via single-sample gene-set enrichment analysis (ssGSEA). The differences were detected using the wilcox.test R package.

Immune cell infiltration in the TME of MCL molecular clusters was revealed by the ImmuneScore, StromalScore, ESTIMATEScore, and TumorPurity using the "ESTIMATE (v1.0.13)" R package. The differences were detected using the wilcox.test R package. Next, the enrichment scores of immune infiltrating cells were calculated by the ssGSEA algorithm via the gene set variation analysis (GSVA) (v1.34.0) R package. In addition, immune cell infiltration was explored using the "CIBERSORT (v1.03)" and "xCell (v1.1.0)" R packages, respectively, and the differences were detected using the wilcox.test R package. The expression levels of familiar immune checkpoint molecules in the distinct MCL molecular clusters were displayed in a boxplot, and the differences were detected using the wilcox.test R package.

Identification of prognostic genes and development of a prognostic risk score model for distinct MCL molecular clusters

The DEGs of distinct MCL molecular clusters in the GSE93291 dataset were obtained using the "limma (v3.42.2)" R package. The threshold was defined as follows: adjusted P<0.05 and |logFC| >1. The prognostic genes were identified via LASSO-Cox analysis, followed by univariate Cox regression analysis of the DEGs that were significantly correlated with the OS of MCL patients, with a cut-off value of P<0.05. The prognostic risk score model was established by the screened prognostic genes using the "glmnet (v4.0-2)" R package via cross-validation for lambda. The minimum of 1-standard error of λ was employed, and the maxit was set to 1,000. The screened prognostic genes with non-zero coefficients were performed by multivariate Cox regression to calculate relative risk scores, using the enter method. The risk score of each sample was calculated using the following formula:

$$\mathrm{RScore}_i = \sum_{j=1}^{n} \exp_{ji} \times \beta_j \quad [1]$$

where exp refers to the expression level of the relative gene, β denotes the regression coefficient (coef) of the relative gene in LASSO regression, Rscore represents the risk score in each sample, *n* is the number of screened prognostic genes, *i* is the sample, and *j* is the gene.

To verify the efficiency of the prognostic risk score model, we performed a Kaplan-Meier survival analysis to compare the difference in OS between the high- and the low-risk score groups, as distinguished by the median Rscore in the GSE93291 dataset. Subsequently, the receiver operating characteristic (ROC) curve and area under the curve (AUC) was used to assess the prognostic model.

Correlation between the screened prognostic genes and immune cell infiltration or immune checkpoint molecules in distinct MCL molecular clusters

The correlation between the screened prognostic genes in the GSE93291 dataset and immune infiltrating cells was demonstrated via Pearson's correlation analysis. In addition, a similar correlation analysis was performed between the prognostic genes and familiar immune checkpoint molecules.

Statistical analysis

Statistical analysis was performed using related R software packages and the bioinformatics databases mentioned above. The Wilcoxon test was utilized to compare two independent non-parametric samples. Survival analysis was performed using the log-rank test. The screened genes correlated with the relative cells or molecules were evaluated using Pearson's correlation test. $P<0.05$ was considered statistically significant.

Results

Expression and enrichment analyses of immune-related genes in MCL

A total of 818 immune-related genes with a relevance score ≥5 were retrieved from the GeneCards database (available at: https://cdn.amegroups.cn/static/public/atm-22-5815-1.xlsx). In the GSE32018 dataset, 722 immune-related genes had available expression data, including 193 DEGs between the MCL tumor and the normal samples (*Figure 2A*, Table S1). In the GSE45717 dataset, 677 immune-related genes had available expression information and there were 211 DEGs (*Figure 2B*, Table S2). There were a total of 77 common DEGs in the GSE32018 and GSE45717 datasets (*Figure 2C*). Functional and pathway enrichment analyses of the common genes showed that they were mainly enriched in T-cell activation, leukocyte cell-cell adhesion, and the regulation of immune cell proliferation via GO analysis of the biological processes (BP); in the external side of the plasma membrane, plasma membrane receptor complex, and the membrane raft via GO analysis of the cellular components (CC); in cytokine receptor binding/activity, cytokine binding/activity, and tumor necrosis factor receptor (superfamily)/major histocompatibility complex (MHC) protein binding via GO analysis of the molecular functions (MF); as well as in cytokine-cytokine receptor interaction, hematopoietic cell lineage, T helper cell 17 (Th17) cell differentiation, T cell receptor signaling pathway, nuclear factor kappa-B (NF-κB) signaling pathway, programmed death-ligand 1 (PD-L1) expression, and the PD-1 checkpoint pathway in cancer via KEGG analysis (*Figure 2D-2G*).

Screening of immune-related hub genes in MCL

By screening the 77 common DEGs, we obtained the immune-related hub genes in MCL using three machine learning algorithms in the GSE32018 dataset. Firstly, the top nine most accurate genes were selected via 10-fold cross-validation by SVM-RFE (*Figure 3A*). The average rankings of the 77 genes are displayed in Table S3. Next, 26 genes were selected via MeanDecreaseGini using a random forest (*Figure 3B,3C*, Table S4). Then, 11 genes with a low mean-squared error were obtained via lasso.min using a LASSO algorithm (*Figure 3D*). Finally, the immune-related hub genes among the three algorithms in MCL were demonstrated using a Venn diagram (*Figure 3E*).

The four common hub genes (*CD247*, *CD3E*, *CD4*, and *GATA3*) were screened for further analyses. PPI network analysis demonstrated an interaction between these genes. GO enrichment analysis revealed that they were mainly enriched in the T-cell receptor signaling pathway (GO:0050852), T-cell selection (GO:0045058), the regulation of interleukin-2 (IL-2) production (GO:0032663), the adaptive immune response (GO:0002250), and cytokine production (GO:0001816). The expression of these four genes exhibited a positive correlation (*Figure 3F,3G*).

The location of the four screened hub genes in the human chromosome is shown in *Figure 4A*. Pearson's correlation analysis indicated that *CD247*, *CD3E*, and *CD4* had a significant positive relationship with $|correlation| >0.6$ (*Figure 4B*). The four hub genes in GSE32018 were also displayed in a volcano plot (*Figure 4C*); the expression of these genes in the tumor samples was markedly lower than that in the normal samples (*Figure 4D,4E*).

Identification of MCL molecular clusters based on the immune-related hub genes in MCL

Two MCL molecular clusters were recognized via a PAC algorithm in the GSE93291 dataset, followed by the unsupervised clustering of the expression matrix of four immune-related hub genes (*Figure 5A-5D*). The MCL patients in molecular cluster 2 had worse OS compared

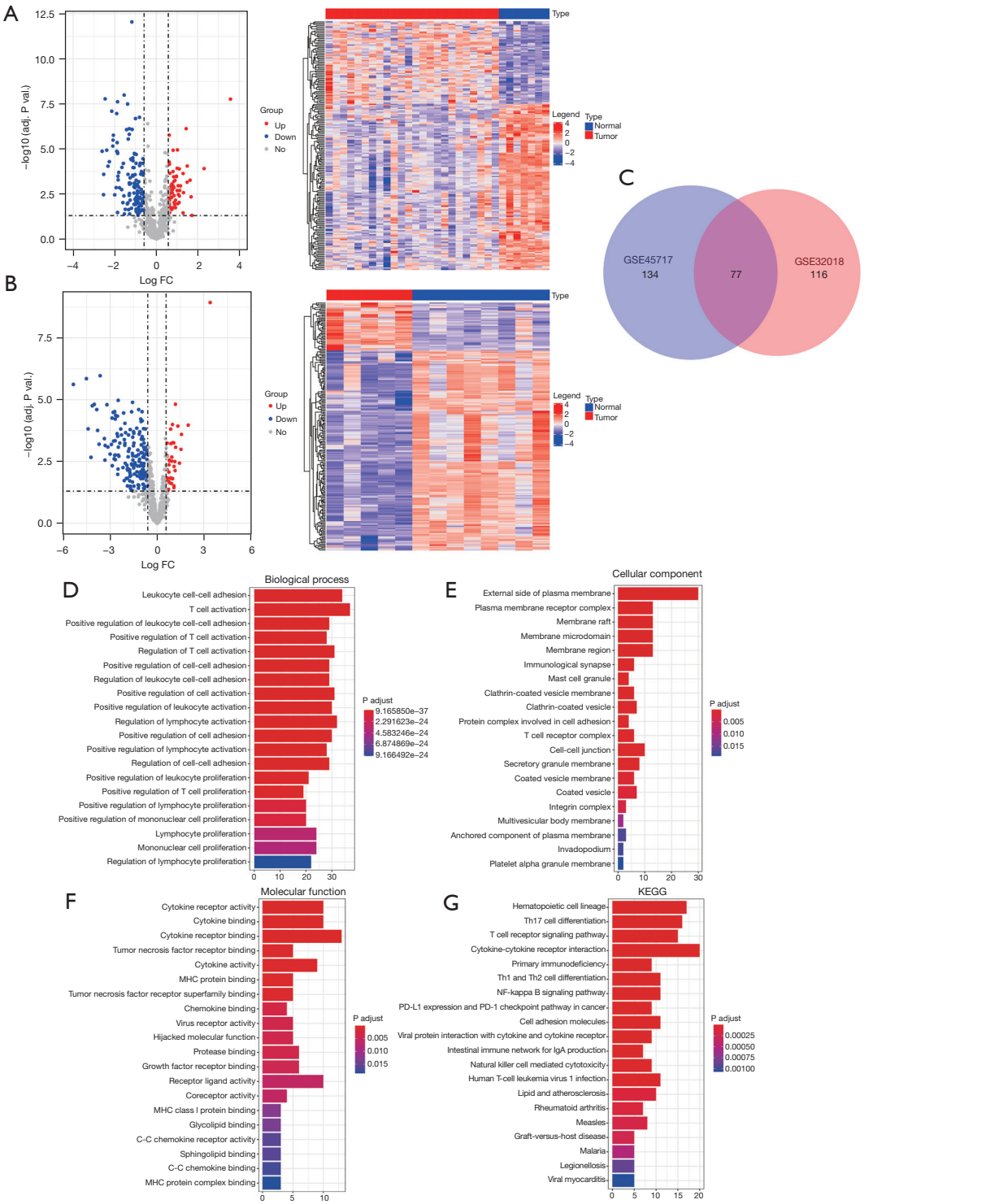

Figure 2 The immune-related genes in MCL. (A,B) Volcano plot and heatmap of 193 DEGs in GSE32018 and 211 DEGs in GSE45717. (C) Venn diagram of DEGs in GSE32018 and GSE45717. (D-F) GO analysis (BP, CC, and MF) of the 77 common genes. (G) KEGG analysis of the 77 common genes. The x-axis in 2D-2G represented –log10 (adjusted P value), respectively. FC, fold change; KEGG, Kyoto Encyclopedia of Genes and Genomes; PD-L1, programmed death-ligand 1; PD-1, programmed death 1; MCL, mantle cell lymphoma; DEGs, differentially expressed genes; GO, Gene Ontology; BP, biological processes; CC, cellular components; MF, molecular functions.

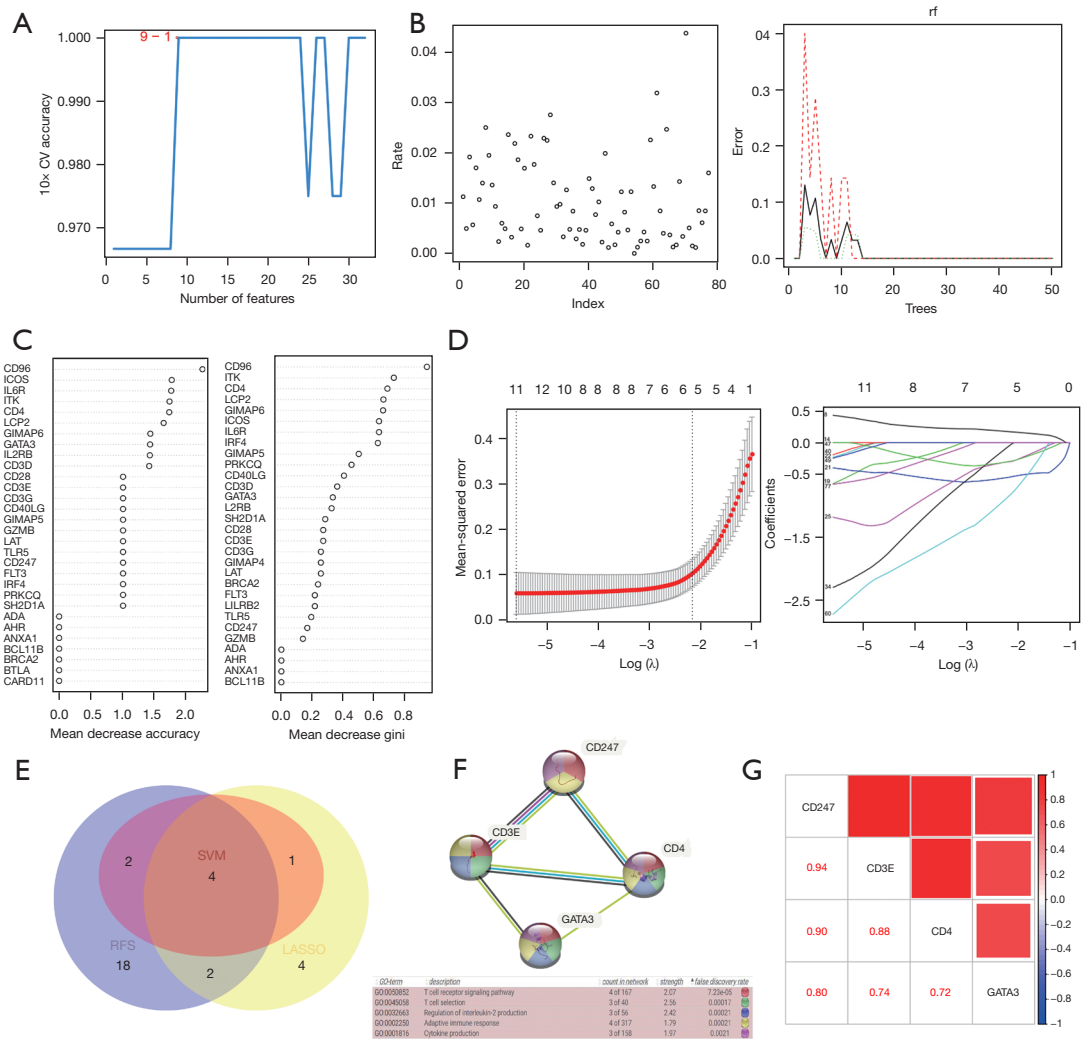

Figure 3 The screening of immune-related hub genes in MCL (GSE32018). (A) The accuracy of the 77 common DEGs by SVM-RFE. (B) Error in the screening process using a random forest algorithm. (C) The MeanDecreaseAccuracy and MeanDecreaseGini of hub genes using a random forest algorithm. (D) The coefficient of lambda and the lambda.min from 10-fold cross-validation using a LASSO algorithm. (E) Venn diagram of hub genes in three machine learning algorithms (SVM, SVM-RFE; RFS). (F) PPI network and GO analysis of the four hub genes. (G) Correlation among the four hub genes. CV, cross-validation; RFS, Random forest; SVM, SVM-RFE, support vector machine-recursive feature elimination; GO, Gene Ontology; MCL, mantle cell lymphoma; DEGs, differentially expressed genes; LASSO, least absolute shrinkage and selection operator; PPI, protein-protein interaction.

with those in cluster 1 (P=0.042) (*Figure 5E*). The overall expression of these hub genes in cluster 2 was lower than that in cluster 1 (*Figure 5F,5G*).

The landscape of immune cell infiltration and immune checkpoint molecules in distinct MCL molecular clusters

A total of 26 out of 50 pathways of hallmark gene sets exhibited differences between the two MCL molecular clusters in the GSE93291 dataset. The top 10 alterative pathways included: APICAL_JUNCTION, APICAL_SURFACE, ALLOGRAFT_REJECTION, WNT_BETA_CATENIN_SIGNALING, IL6_JAK_STAT3_SIGNALING, INTERFERON_GAMMA_RESPONSE, HEDGEHOG_SIGNALING, MYC_TARGETS_V1, INFLAMMATORY_RESPONSE, and OXIDATIVE_

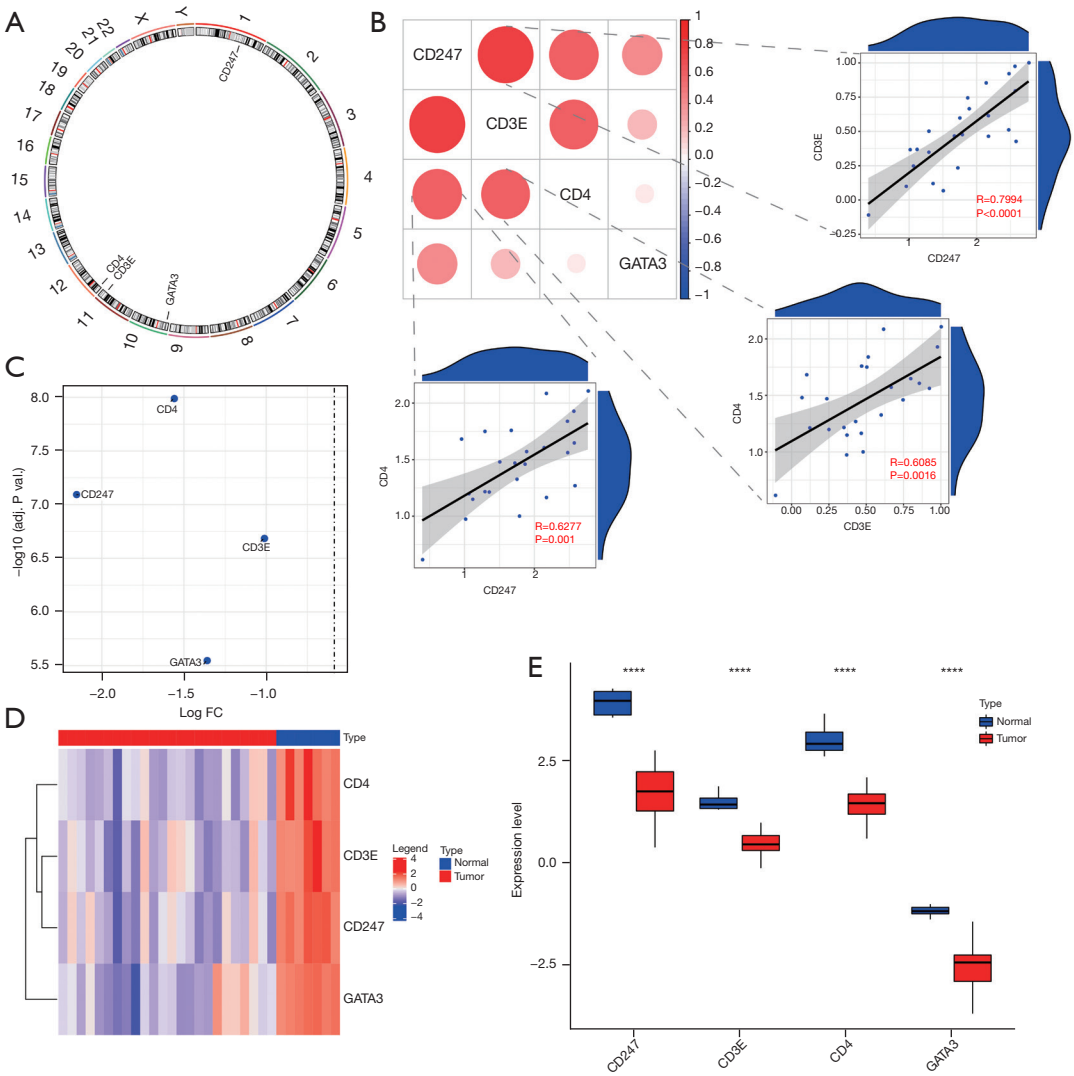

Figure 4 The landscape of immune-related hub genes in MCL (GSE32018). (A) The chromosome location of the four hub genes. (B) Correlation among the hub genes. (C) Volcano plot of the hub genes. (D,E) Expression of the hub genes in the tumor and normal samples. ****, P<0.0001. FC, fold change; MCL, mantle cell lymphoma.

PHOSPHORYLATION (*Figure 6A*).

Compared with those in cluster 1, the ImmuneScore and ESTIMATEScore were lower in the cluster 2 group, while the TumorPurity scores were higher (*Figure 6B,6C*). A total of 18 of 28 immune cell infiltrations in the TME had different scores between the two clusters. The activated $CD8^+$ T cell, activated dendritic cell, natural killer T cell, and T follicular helper cell scores in cluster 2 were significantly lower than that in cluster 1 (*Figure 6D*). Similar differences were observed in the immune cell proportion of two clusters, which were analyzed by CIBERSORT and xCell, respectively (Figure S1A,S1B).

Forty-one of the 63 familiar immune checkpoint molecules had available expression information in the GSE93291 dataset (Table S5). The data showed that 25 immune checkpoint molecules had different expression levels in the two MCL clusters. Compared with cluster 1, only *CD86* was higher in cluster 2, while the other 24 molecules were lower, especially *BTN3A1*, *BTN3A2*, *BTN3A3*, *CD200*, *CD274*, *CD28*, *ICOS*, *IDO1*, *IL2RB*, and

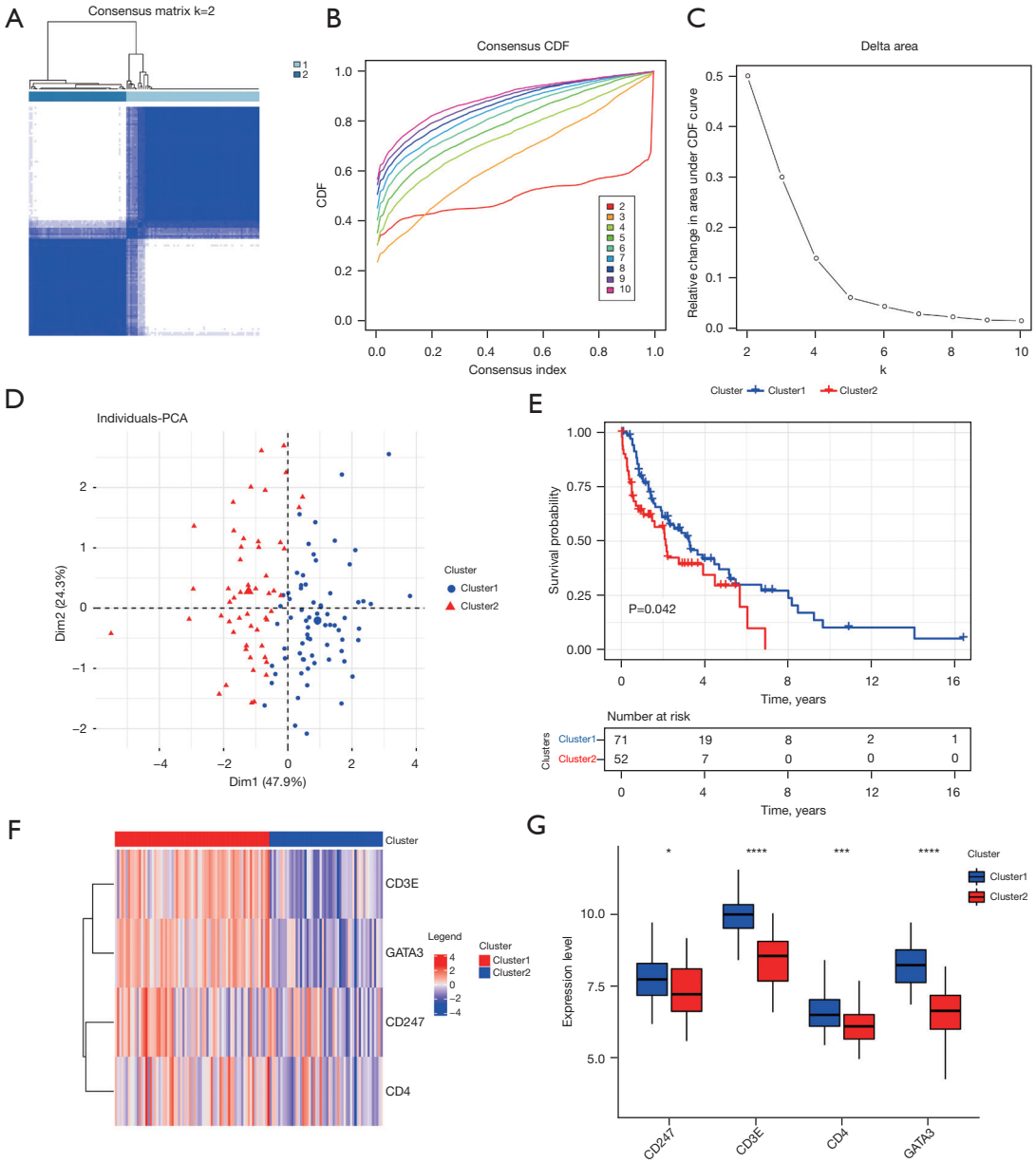

Figure 5 Identification of MCL molecular clusters in MCL (GSE93291). (A-C) Two MCL molecular clusters were classified by unsupervised clustering and displayed using a heatmap, CDF plot, and macadam plot. (D) Analysis of MCL samples in two clusters by PCA. (E) Prognostic OS differences between the two clusters. (F,G) Expression of the four immune-related hub genes in the two clusters. ****, P<0.0001; ***, P<0.001; *, P<0.05. CDF, cumulative distribution function; PCA, principal component analysis; MCL, mantle cell lymphoma; OS, overall survival.

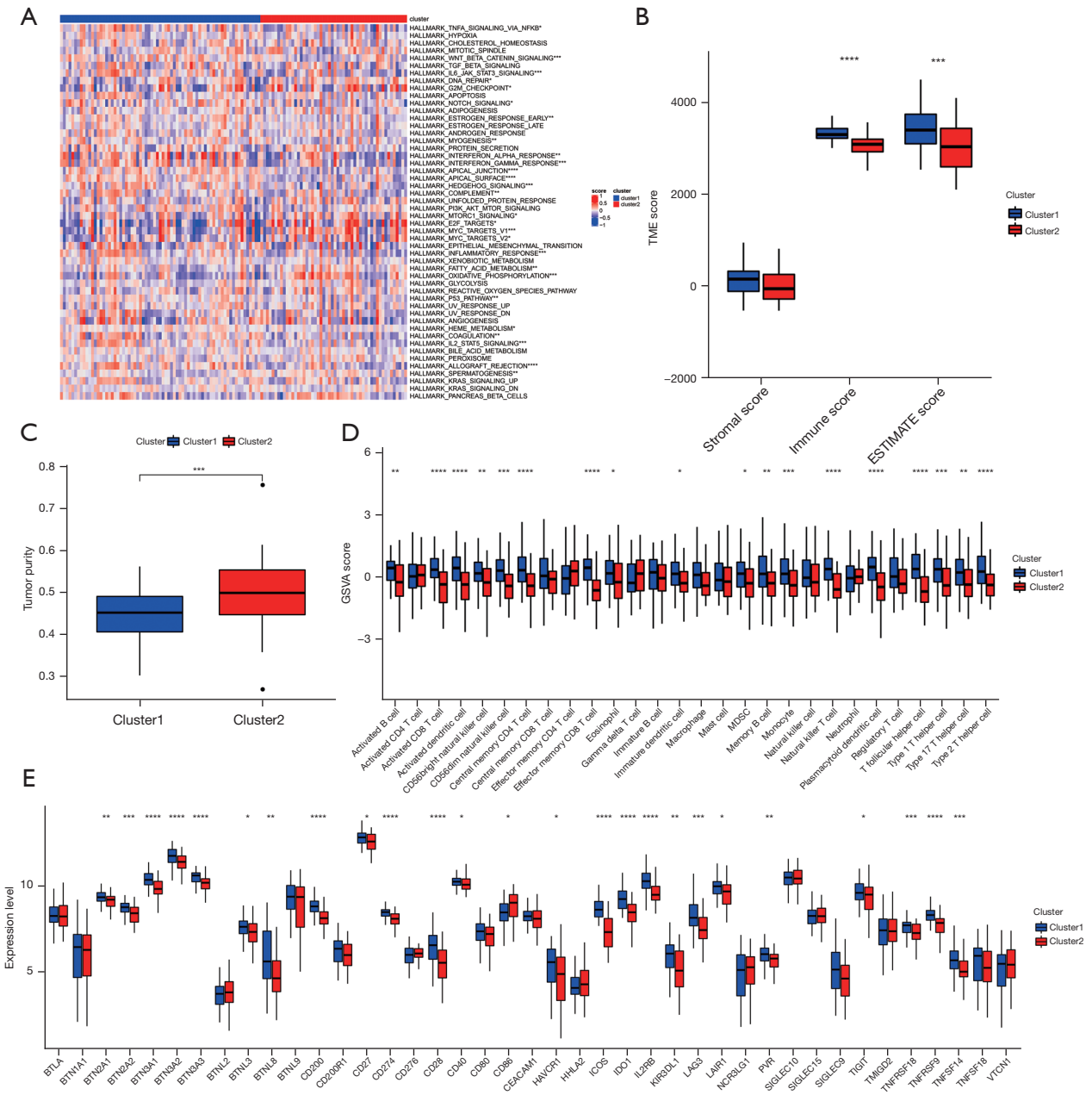

Figure 6 The landscape of immune cell infiltration and immune checkpoint molecules in the MCL molecular clusters (GSE93291). (A) Enrichment analysis of the pathways of hallmark gene sets in the two MCL clusters. (B,C) The ImmuneScore, StromalScore, ESTIMATEScore, and TumorPurity scores in the MCL samples of the two clusters. (D) The scores of 28 immune cell infiltrations in the TME of the two clusters were calculated by ssGSEA via GSVA. (E) The expression of 41 immune checkpoint molecules in the two clusters. ****, P<0.0001; ***, P<0.001; **, P<0.01; *, P<0.05. TME, tumor microenvironment; MCL, mantle cell lymphoma; ssGSEA, single-sample gene-set enrichment analysis; GSVA, gene set variation analysis.

TNFRSF9 (*Figure 6E*).

Identification of the prognostic genes and development of the prognostic risk score model for distinct MCL molecular clusters

In order to explore the prognostic DEGs of the two MCL molecular clusters, the 65 DEGs of the two clusters and coding relative proteins were obtained in the GSE93291 dataset (Table S6), and the 20 DEGs significantly associated with the OS of MCL patients were screened by univariate Cox regression analysis (Table S7). Then, six DEGs (*LGALS2*, *LAMP3*, *ICOS*, *FCAMR*, *IGFBP4*, and *C1QA*) were selected to establish the prognostic risk score model via LASSO-Cox analysis (*Figure 7A-7C*). The poor OS was related to the increased *IGFBP4* and *C1QA* expression groups; however, it was more likely to occur in the low *LGALS2*, *LAMP3*, *ICOS*, and *FCAMR* expression groups (P<0.05). The following formula was used: Risk Score = *LGALS2* × (–0.1746) + *LAMP3* × (–0.1413) + *ICOS* × (–0.1352) + *FCAMR* × (–0.1327) + *IGFBP4* × 0.0356 + *C1QA* × 0.1987. MCL patients who had a higher prognostic model risk score had a poorer prognosis, as verified by Kaplan-Meier survival analysis (P<0.0001) (*Figure 7D*). The AUCs at 1, 3, and 5 years were 0.8, 0.79, and 0.7, respectively (*Figure 7E*). Taken together, these results demonstrated that the prognostic model had a prominent efficiency.

Correlation between the screened prognostic genes and immune cell infiltration or immune checkpoint molecules for distinct MCL molecular clusters

The six screened prognostic genes (*LGALS2*, *LAMP3*, *ICOS*, *FCAMR*, *IGFBP4*, and *C1QA*) were correlated with the majority of the 28 immune infiltrating cells. Immune cells that were significantly positively correlated with the whole six prognostic genes were activated in $CD8^+$ T cells, effector memory $CD8^+$ T cells, natural killer T cells, and type 1 T helper cells. *IGFBP4* was negatively correlated with effector memory $CD4^+$ T cells and gamma delta T cells, while *C1QA* was negatively correlated with immature B cells (*Figure 8A*). Most of the immune checkpoint molecules were also correlated with the six prognostic genes. Also, a significant positive correlation with the whole six prognostic genes was observed in *ICOS*, *CD200*, *TNFRSF9*, *IL2RB*, *CD274*, and *BTN3A1* (*Figure 8B*).

Discussion

In the present study, we initially compared 77 immune-related differentially expressed genes (DEGs) in MCL samples with normal controls in both the GSE32018 and GSE45717 datasets. These genes were mainly enriched in T-cell activation, the plasma membrane, and cytokine receptor binding and activity by GO analysis, and in a series of pathways by KEGG analysis, including cytokine-cytokine receptor interaction and the NF-kappa B signaling pathway. A previous study showed that these two pathways were enriched in DEGs both in the GSE32018 and GSE9327 datasets, which used normal and reactive lymph nodes as controls, respectively (22). This indicates that the enriched pathways in DEGs between tumor samples and controls might be a reason for the selection of targeted agents in MCL, such as bortezomib interfering with the NF-kappa B signaling pathway (1).

We then screened four common hub genes (*CD247*, *CD3E*, *CD4*, and *GATA3*) using three machine learning algorithms: SVM-RFE, random forest, and LASSO. Previous studies have revealed the biological functions and application prospects of these genes. *CD247*, which encodes the CD3ζ protein, regulates the immune response and participates in tumorigenesis (23). *CD3E*, which encodes the CD3-epsilon polypeptide, is a built-in multifunctional signal tuner in T-cell development (24). *CD4*, which encodes the CD4 membrane glycoprotein, assists the germinal center reaction and contributes to the activation, functions, and longevity of $CD8^+$ T-cells and B-cells (25). *GATA3*, which encodes a protein of the GATA family of transcription factors, is an important regulator of T-cell development and may be a biomarker associated with poor prognosis in distinct subtypes of nodal peripheral T-cell lymphoma (26). We found that the hub genes were mainly enriched in the T-cell receptor signaling pathway, T-cell selection, the regulation of IL-2 production, the adaptive immune response, and cytokine production. These relative pathways were consistent with previous research (22). Moreover, *CD247*, *CD3E*, and *CD4* exhibited a positive relationship with each other. Also, the whole expression of hub genes in MCL was significantly lower than that in the normal samples. These findings suggested that the reduced expression of the four immune-related hub genes, which were related to a series of immune signaling pathways, might participate in MCL tumor progression.

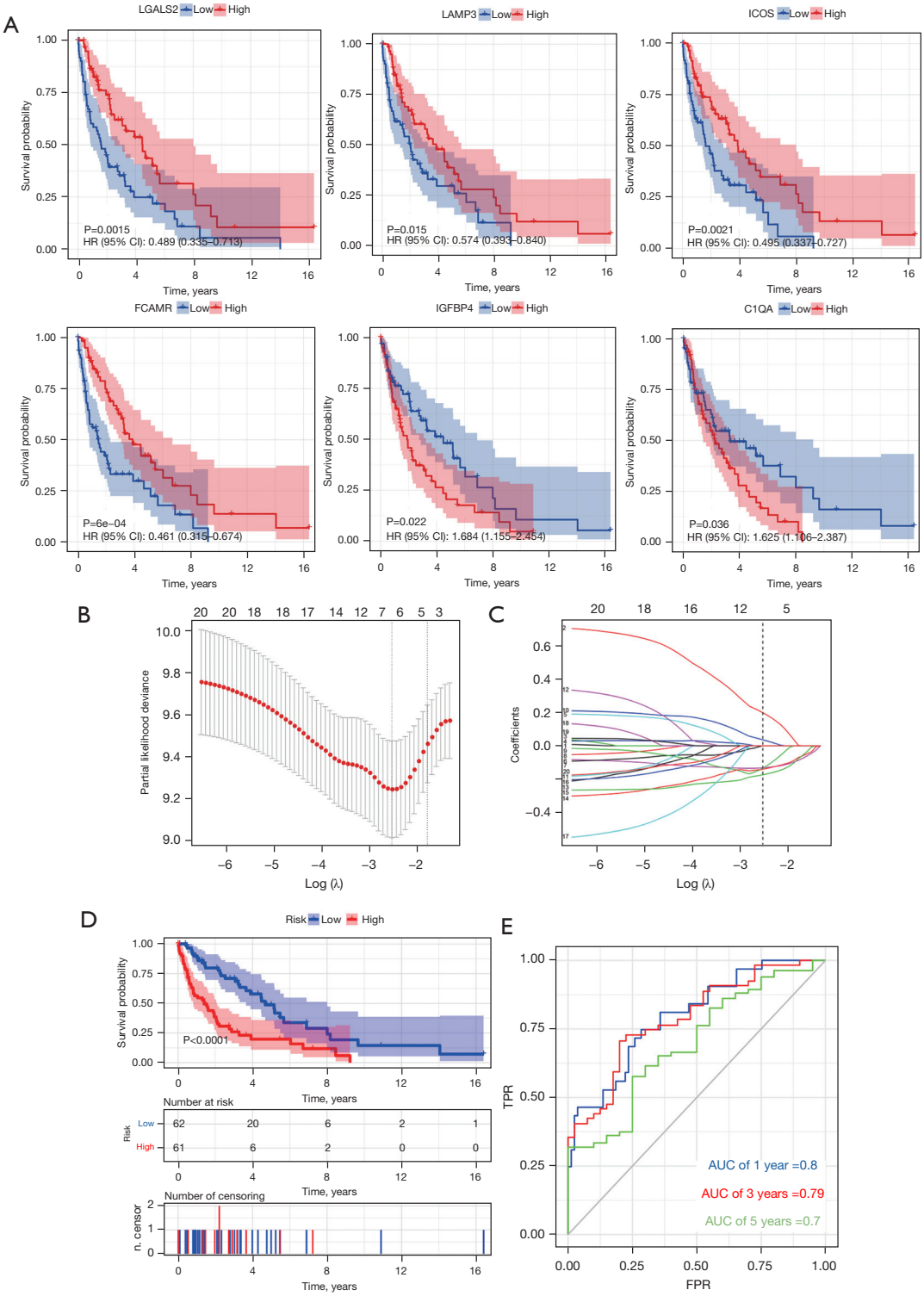

Figure 7 The prognostic genes and prognostic risk score model for the MCL molecular clusters (GSE93291). (A) Prognostic value of the expression of six DEGs (*LGALS2*, *LAMP3*, *ICOS*, *FCAMR*, *IGFBP4*, and *C1QA*) in the MCL samples. (B,C) The prognostic risk score model was established by LASSO-Cox analysis. (D,E) The efficiency of the prognostic model was verified by Kaplan-Meier and ROC curve analysis. HR, hazard ratio; AUC, area under the curve; TPR, true positive rate; FPR, false positive rate; MCL, mantle cell lymphoma; LASSO, least absolute shrinkage and selection operator; ROC, receiver operating characteristic.

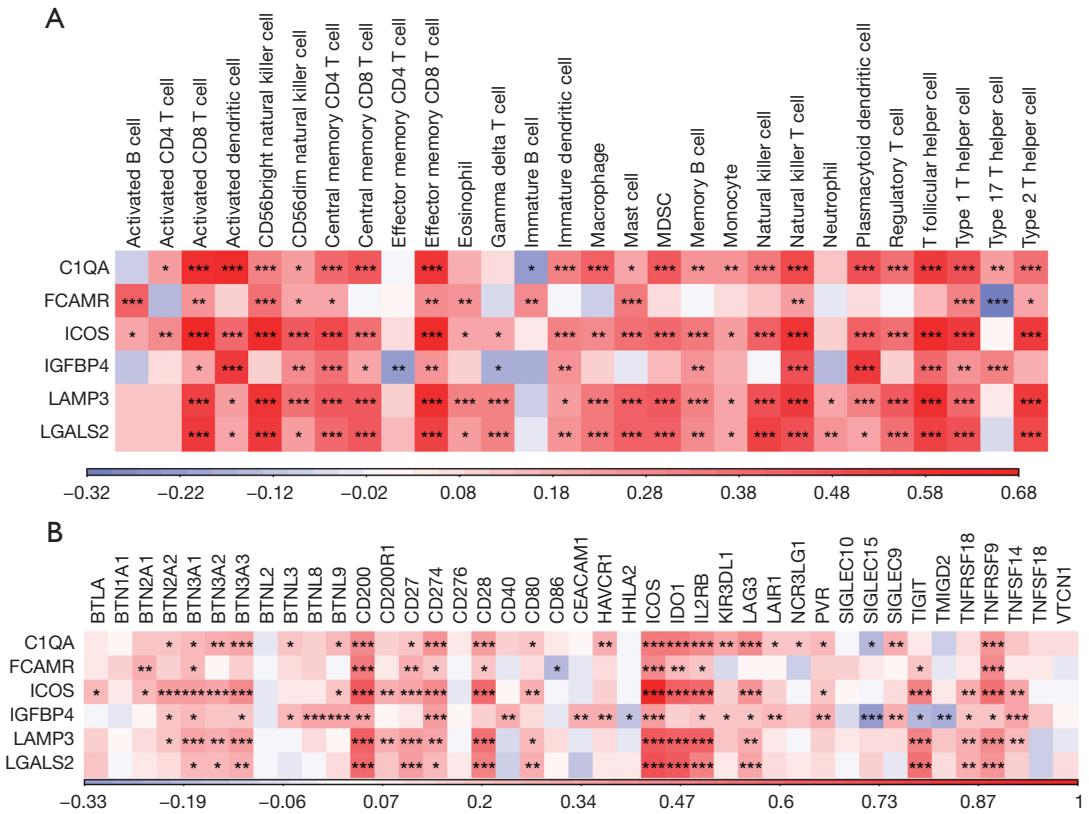

Figure 8 Correlation between the screened prognostic genes and the immune infiltrating cells or immune checkpoint molecules in MCL (GSE93291). (A,B) The correlation between the six prognostic genes and the immune infiltrating cells or immune checkpoint molecules. ***, P<0.001; **, P<0.01; *, P<0.05. MCL, mantle cell lymphoma.

A previous study observed that fewer immune escape genes, which are significantly expressed in diffuse large B-cell lymphoma and follicular lymphoma, were enriched in MCL samples (27). To further identify the four screened hub genes, we utilized unsupervised clustering of the expression matrix of hub genes and recognized two MCL molecular clusters in the much larger GSE93291 dataset. Interestingly, the patients in cluster 2 had a significantly worse OS and lower expression of the whole hub genes, compared with those in cluster 1. This indicated that the down-regulated expression of the four hub genes was unfavorable to the prognosis of MCL patients. Furthermore, we explored the landscape of immune cell infiltration and immune checkpoint molecules in the two MCL clusters. Several different pathways of hallmark gene sets were explored between the two clusters. The results were consistent with previous research on the immune landscape of MCL in terms of the cytolytic score-related pathways, including INTERFERON_GAMMA_RESPONSE, ALLOGRAFT_REJECTION, and INFLAMMATORY_RESPONSE (12). However, using the different classification methods from a recent study, which classified MCL into four clusters by whole-exome sequencing and relatively matched RNA sequencing (RNA-Seq) data analysis (8), we also found that the active MYC pathway was involved in the MCL progression.

Moreover, we observed that several immune scores reflecting the immune cell infiltration in the TME were different between the two MCL clusters. In cluster 2, the activated $CD8^+$ T-cells, activated dendritic cells, natural killer T cells, and T follicular helper cells exhibited significantly lower scores. This indicated that a variety of activated immune effector cells were lower in cluster 2. Previous studies have shown that the various characteristics of immune cell infiltration affected MCL outcomes. Zhang *et al.* discovered the progressive dampening of $CD8^+$ T cells in refractory MCL patients (28). The low absolute $CD4^+$ T cell counts in peripheral blood were a significant predictor

of unfavorable OS in MCL patients, regardless of whether they received rituximab treatment (29). Similarly, we found that central memory $CD4^+$ T cells were decreased in cluster 2, with a poor outcome. Rodrigues *et al.* reported that the infiltrations of CD163-, PD-L1-, and FoxP3-positive cells were indicative of a worse outcome in MCL patients, independent of established risk factors (30).

In this study, only *CD86* was higher among the 25 differentially expressed immune checkpoint molecules in cluster 2, as compared with cluster 1. Also the most significantly decreased molecules were *BTN3A1*, *BTN3A2*, *BTN3A3*, *CD200*, *CD274*, *CD28*, *ICOS*, *IDO1*, *IL2RB*, and *TNFRSF9*. Previous studies have evaluated the expression of several immune checkpoint molecules and explored their effects on the prognosis of MCL and other B-cell lymphomas. The addition of heterodimeric BTN2A1 and BTN3A1 could promote granzyme B-mediated killing of $CD19^+$ lymphoma cells when co-cultured with $V\gamma9V\delta2^+$ T cells (31). Also, CD200 expression in MCL indicated a better prognosis and was associated with CD23 expression, frequent immunoglobulin heavy chain variable region (IGHV) mutations, and the absence of SOX11 expression (32,33). The majority of MCL patients had no or low expression of PD-1 and PD-L1 (14), while co-culturing of primary MCL cells with T-cells could induce PD-L1 surface expression (34). The generation of Tregs, which is a key role in the pathogenesis of follicular lymphoma, was associated with inducible costimulator (ICOS)/ ICOS Ligand (ICOSL) engagement (35). *IL2RB*, which is regarded as a hub gene, might be related to the pathogenesis and prognosis of MCL, as determined by the top-weighted network analysis performed in the GSE93291 dataset (6). *TNFRSF9* and its ligand *TNFSF9* were applied to trigger innate immune activation, involving therapies such as chimeric antigen receptor (CAR) T-cells and bispecific T-cell engagers in MCL and other B-cell lymphomas (36). Therefore, further investigations are needed to examine how the immune checkpoint molecules contribute to the pathogenesis of MCL and evaluate the value of these molecules.

A series of prognostic genes in MCL have been identified (5-7). However, the clinical application of these potential biomarkers as new targets in MCL treatment requires further exploration. In this study, we selected six DEGs (*LGALS2*, *LAMP3*, *ICOS*, *FCAMR*, *IGFBP4*, and *C1QA*) in two MCL clusters, which are associated with OS, to establish an efficient prognostic risk score model. Poor OS was related to increased *IGFBP4* and *C1QA* expression, while the worse prognosis was more likely to occur with low *LGALS2*, *LAMP3*, *ICOS*, and *FCAMR* expression. Also, patients with higher prognostic model risk scores had a markedly poor prognosis. The six prognostic genes directly and indirectly participated in the immune response in numerous tumors, for instance, *LGALS2* in triple-negative breast cancer (37), *LAMP3*+ dendritic cells in nasopharyngeal carcinomas (38), *ICOS* in the generation of Tregs in follicular lymphoma (35), *FCAMR* in lung squamous cell carcinoma (39), *IGFBP4* in ewing's sarcoma (40), *C1QA* in skin cutaneous melanoma (41). A previous study has suggested that *IGFBP4* is associated with poor outcomes in glioblastoma (42). Interestingly, in diffuse large B cell lymphoma (DLBCL) patients, the *C1qA*[276] polymorphism of the A/A allele is an independent favorable prognostic factor for rituximab plus cyclophosphamide, doxorubicin, vincristine, and prednisone (R-CHOP) as first-line therapy (43), while the expression level of *LGALS2* was not associated with OS but was lower in tumors than in normal samples (44). *LAMP3* is over-expressed in various tumors and is correlated with the poor or good prognosis of different patients (45). The different prognostic effects of these genes might relate to the different types of tumors, although their exact roles and mechanisms in MCL should be further explored.

We also performed Pearson's correlation analysis to assess the relative immune cells and immune checkpoint molecules of the above six prognostic genes. Most types of immune cells were positively correlated with the genes, including activated $CD8^+$ T cells, effector memory $CD8^+$ T cells, natural killer T cells, etc. Meanwhile, effector memory $CD4^+$ T cells and γδT cells exhibited a negative correlation with *IGFBP4*, and immature B cells were negatively correlated with *C1QA*. It is known that γδT cells can produce abundant cytokines and exert a therapeutic response against infection, autoimmunity, and cancer (46). The modulation of immune cells correlated with the six prognostic genes might explain the regulatory mechanisms in the TME of MCL to some extent. As for the immune checkpoint molecules, *ICOS*, *CD200*, *TNFRSF9*, *IL2RB*, *CD274*, and *BTN3A1* displayed significantly positive correlations with the whole six prognostic genes. Taken together, these findings suggested that the accommodation of immune checkpoint molecules might participate in the pathogenesis of MCL.

Conclusions

In conclusion, we screened four immune-related hub genes

(*CD247*, *CD3E*, *CD4*, and *GATA3*) in MCL, which were mainly enriched in the T-cell receptor signaling pathway and exhibited lower expression in tumors compared with normal samples. Subsequently, we recognized two MCL molecular clusters based on the hub genes. Patients in cluster 2 had a significantly worse OS compared with those in cluster 1; the hub genes were down-regulated, a variety of activated immune effector cells declined, and the majority of immune checkpoint molecules decreased. Moreover, we established an efficient prognostic risk score model using six prognostic genes (*LGALS2*, *LAMP3*, *ICOS*, *FCAMR*, *IGFBP4*, and *C1QA*) that were differentially expressed between the two MCL clusters. Patients with higher prognostic model risk scores had a significantly poorer prognosis. Although several biomarkers for the prognosis of MCL patients have been reported, few researches focused on the immune-related prognostic genes and the prognostic model developed by the DEGs of immune-related molecular clusters of MCL. This study suggested that these immune-related hub genes, the modulated immune cells, and the immune checkpoint molecules might be involved in oncogenesis and could be prognostic biomarkers in MCL. These immune-related biomarkers (four immune-related hub genes, six prognostic genes, and the relative molecules) will enrich the prognostic scoring system of MCL and provide preliminary basis for the clinical application of immunotherapy, including the immune checkpoint blockade therapies.

Further research should be carried out to examine the regulatory mechanisms through which the immune-related hub genes contribute to tumorigenesis, verify the efficiency of the prognostic model in larger MCL cohorts, and explore potential therapeutic targets that enhance the effect of immunotherapy.

Acknowledgments

We are very grateful for the assistance from Professor Jian-Quan Chen in the Central Laboratory and Translational Medicine Research Center of the Affiliated Jiangning Hospital of Nanjing Medical University.

Funding: This study was supported by the Natural Science Foundation of Jiangsu Province for Youths (No. BK20180280); the Innovation and Entrepreneurship Foundation of Jiangsu Province for Doctor (No. JSSCBS20211612); the Science and Technology Development Foundation for Health of Nanjing (Nos. YKK21227 and YKK20200); the Youth Innovation Foundation of the Affiliated Jiangning Hospital of Nanjing Medical University (Nos. JNYYZXKY202021 and JNYYZXKY202121); the Scientific Research Foundation of the Affiliated Jiangning Hospital of Nanjing Medical University for PhD. (No. JNYYRC202101); and the Science and Technology Development for Social Undertakings Foundation of the Jiangning district in Nanjing (No. 2020SHSY0101).

Footnote

Reporting Checklist: The authors have completed the TRIPOD reporting checklist. Available at https://atm.amegroups.com/article/view/10.21037/atm-22-5815/rc

Conflicts of Interest: All authors have completed the ICMJE uniform disclosure form (available at https://atm.amegroups.com/article/view/10.21037/atm-22-5815/coif). The authors have no conflicts of interest to declare.

Ethical Statement: The authors are accountable for all aspects of the work in ensuring that questions related to the accuracy or integrity of any part of the work are appropriately investigated and resolved. The study was conducted in accordance with the Declaration of Helsinki (as revised in 2013).

References

1. Armitage JO, Longo DL. Mantle-Cell Lymphoma. N Engl J Med 2022;386:2495-506.
2. Herrmann A, Hoster E, Zwingers T, et al. Improvement of overall survival in advanced stage mantle cell lymphoma. J Clin Oncol 2009;27:511-8.
3. Eyre TA, Cheah CY, Wang ML. Therapeutic options for relapsed/refractory mantle cell lymphoma. Blood 2022;139:666-77.
4. Ladha A, Zhao J, Epner EM, et al. Mantle cell lymphoma and its management: where are we now? Exp Hematol

Oncol 2019;8:2.
5. Bomben R, Ferrero S, D'Agaro T, et al. A B-cell receptor-related gene signature predicts survival in mantle cell lymphoma: results from the Fondazione Italiana Linfomi MCL-0208 trial. Haematologica 2018;103:849-56.
6. Guo D, Wang H, Sun L, et al. Identification of key gene modules and hub genes of human mantle cell lymphoma by coexpression network analysis. PeerJ 2020;8:e8843.
7. Carreras J, Nakamura N, Hamoudi R. Artificial Intelligence Analysis of Gene Expression Predicted the Overall Survival of Mantle Cell Lymphoma and a Large Pan-Cancer Series. Healthcare (Basel) 2022;10:155.
8. Yi S, Yan Y, Jin M, et al. Genomic and transcriptomic profiling reveals distinct molecular subsets associated with outcomes in mantle cell lymphoma. J Clin Invest 2022;132:e153283.
9. Kraehenbuehl L, Weng CH, Eghbali S, et al. Enhancing immunotherapy in cancer by targeting emerging immunomodulatory pathways. Nat Rev Clin Oncol 2022;19:37-50.
10. Ansell SM, Lesokhin AM, Borrello I, et al. PD-1 blockade with nivolumab in relapsed or refractory Hodgkin's lymphoma. N Engl J Med 2015;372:311-9.
11. Li X, Cheng Y, Zhang M, et al. Activity of pembrolizumab in relapsed/refractory NK/T-cell lymphoma. J Hematol Oncol 2018;11:15.
12. Dufva O, Pölönen P, Brück O, et al. Immunogenomic Landscape of Hematological Malignancies. Cancer Cell 2020;38:380-399.e13.
13. Xu-Monette ZY, Zhou J, Young KH. PD-1 expression and clinical PD-1 blockade in B-cell lymphomas. Blood 2018;131:68-83.
14. Ameli F, Shajareh E, Mokhtari M, et al. Expression of PD1 and PDL1 as immune-checkpoint inhibitors in mantle cell lymphoma. BMC Cancer 2022;22:848.
15. Assis-Mendonça GR, Fattori A, Rocha RM, et al. Single nucleotide variants in immune-response genes and the tumor microenvironment composition predict progression of mantle cell lymphoma. BMC Cancer 2021;21:209.
16. Papin A, Tessoulin B, Bellanger C, et al. CSF1R and BTK inhibitions as novel strategies to disrupt the dialog between mantle cell lymphoma and macrophages. Leukemia 2019;33:2442-53.
17. Chen Z, Teo AE, McCarty N. ROS-Induced CXCR4 Signaling Regulates Mantle Cell Lymphoma (MCL) Cell Survival and Drug Resistance in the Bone Marrow Microenvironment via Autophagy. Clin Cancer Res 2016;22:187-99.
18. Lv H, Fei Y, Li W, et al. A novel clinical immune-related prognostic model predicts the overall survival of mantle cell lymphoma. Hematol Oncol 2022;40:343-55.
19. Gómez-Abad C, Pisonero H, Blanco-Aparicio C, et al. PIM2 inhibition as a rational therapeutic approach in B-cell lymphoma. Blood 2011;118:5517-27.
20. Espinet B, Ferrer A, Bellosillo B, et al. Distinction between asymptomatic monoclonal B-cell lymphocytosis with cyclin D1 overexpression and mantle cell lymphoma: from molecular profiling to flow cytometry. Clin Cancer Res 2014;20:1007-19.
21. Scott DW, Abrisqueta P, Wright GW, et al. New Molecular Assay for the Proliferation Signature in Mantle Cell Lymphoma Applicable to Formalin-Fixed Paraffin-Embedded Biopsies. J Clin Oncol 2017;35:1668-77.
22. Yan W, Li SX, Wei M, et al. Identification of MMP9 as a novel key gene in mantle cell lymphoma based on bioinformatic analysis and design of cyclic peptides as MMP9 inhibitors based on molecular docking. Oncol Rep 2018;40:2515-24.
23. Dexiu C, Xianying L, Yingchun H, et al. Advances in CD247. Scand J Immunol 2022;96:e13170.
24. Wu W, Zhou Q, Masubuchi T, et al. Multiple Signaling Roles of CD3epsilon and Its Application in CAR-T Cell Therapy. Cell 2020;182:855-71.
25. Lisco A, Ye P, Wong CS, et al. Lost in Translation: Lack of CD4 Expression due to a Novel Genetic Defect. J Infect Dis 2021;223:645-54.
26. de Pádua Covas Lage LA, Brito CV, Levy D, et al. Diagnostic and prognostic implications of tumor expression of the GATA-3 gene in nodal peripheral T-cell lymphoma (nPTCL): Retrospective data from a Latin American cohort. Leuk Res 2022;114:106794.
27. Tosolini M, Algans C, Pont F, et al. Large-scale microarray profiling reveals four stages of immune escape in non-Hodgkin lymphomas. Oncoimmunology 2016;5:e1188246.
28. Zhang S, Jiang VC, Han G, et al. Longitudinal single-cell profiling reveals molecular heterogeneity and tumor-immune evolution in refractory mantle cell lymphoma. Nat Commun 2021;12:2877.
29. Zhang XY, Xu J, Zhu HY, et al. Negative prognostic impact of low absolute CD4(+) T cell counts in peripheral blood in mantle cell lymphoma. Cancer Sci 2016;107:1471-6.
30. Rodrigues JM, Nikkarinen A, Hollander P, et al. Infiltration of CD163-, PD-L1- and FoxP3-positive cells adversely affects outcome in patients with mantle cell lymphoma independent of established risk factors. Br J

Haematol 2021;193:520-31.
31. Lai AY, Patel A, Brewer F, et al. Cutting Edge: Bispecific γδ T Cell Engager Containing Heterodimeric BTN2A1 and BTN3A1 Promotes Targeted Activation of Vγ9Vδ2+ T Cells in the Presence of Costimulation by CD28 or NKG2D. J Immunol 2022;209:1475-80.
32. Hu Z, Sun Y, Schlette EJ, et al. CD200 expression in mantle cell lymphoma identifies a unique subgroup of patients with frequent IGHV mutations, absence of SOX11 expression, and an indolent clinical course. Mod Pathol 2018;31:327-36.
33. Saksena A, Yin CC, Xu J, et al. CD23 expression in mantle cell lymphoma is associated with CD200 expression, leukemic non-nodal form, and a better prognosis. Hum Pathol 2019;89:71-80.
34. Harrington BK, Wheeler E, Hornbuckle K, et al. Modulation of immune checkpoint molecule expression in mantle cell lymphoma. Leuk Lymphoma 2019;60:2498-507.
35. Le KS, Thibult ML, Just-Landi S, et al. Follicular B Lymphomas Generate Regulatory T Cells via the ICOS/ICOSL Pathway and Are Susceptible to Treatment by Anti-ICOS/ICOSL Therapy. Cancer Res 2016;76:4648-60.
36. Watanabe T. Approaches of the Innate Immune System to Ameliorate Adaptive Immunotherapy for B-Cell Non-Hodgkin Lymphoma in Their Microenvironment. Cancers (Basel) 2021;14:141.
37. Ji P, Gong Y, Jin ML, et al. In vivo multidimensional CRISPR screens identify Lgals2 as an immunotherapy target in triple-negative breast cancer. Sci Adv 2022;8:eabl8247.
38. Peng WS, Zhou X, Yan WB, et al. Dissecting the heterogeneity of the microenvironment in primary and recurrent nasopharyngeal carcinomas using single-cell RNA sequencing. Oncoimmunology 2022;11:2026583.
39. Li N, Wang J, Zhan X. Identification of Immune-Related Gene Signatures in Lung Adenocarcinoma and Lung Squamous Cell Carcinoma. Front Immunol 2021;12:752643.
40. Zhou Y, Xu B, Wu S, et al. Prognostic Immune-Related Genes of Patients With Ewing's Sarcoma. Front Genet 2021;12:669549.
41. Yang H, Che D, Gu Y, et al. Prognostic and immune-related value of complement C1Q (C1QA, C1QB, and C1QC) in skin cutaneous melanoma. Front Genet 2022;13:940306.
42. Zhong Z, Xu X, Han S, et al. Comprehensive Analysis of Prognostic Value and Immune Infiltration of IGFBP Family Members in Glioblastoma. J Healthc Eng 2022;2022:2929695.
43. Jin X, Ding H, Ding N, et al. Homozygous A polymorphism of the complement C1qA276 correlates with prolonged overall survival in patients with diffuse large B cell lymphoma treated with R-CHOP. J Hematol Oncol 2012;5:51.
44. Ma C, Li H. Hub Gene and Its Key Effects on Diffuse Large B-Cell Lymphoma by Weighted Gene Coexpression Network Analysis. Biomed Res Int 2021;2021:8127145.
45. Alessandrini F, Pezzè L, Ciribilli Y. LAMPs: Shedding light on cancer biology. Semin Oncol 2017;44:239-53.
46. Muro R, Takayanagi H, Nitta T. T cell receptor signaling for γδT cell development. Inflamm Regen 2019;39:6.

(English Language Editor: A. Kassem)

Cite this article as: Zhang W, Shi JN, Wang HN, Zhang T, Zhou X, Zhang HM, Zhu F. Identification of immune-related genes and development of a prognostic model in mantle cell lymphoma. Ann Transl Med 2022;10(24):1323. doi: 10.21037/atm-22-5815

Table S1 The 193 differentially expressed immune-related genes between the tumor and normal samples (GSE32018)

	ID	logFC	AveExpr	t	P.Value	adj.P.Val	B
CCND1	NA	3.560162	0.433423	9.77536	4.98E-11	1.74E-08	15.21051
CD28	NA	-2.62568	0.149047	-6.39063	3.89E-07	1.35E-05	6.428437
CTSG	NA	-2.5571	0.852059	-3.87416	0.000512	0.00348	-0.57031
AICDA	NA	-2.54907	1.444855	-5.05673	1.78E-05	0.000259	2.68189
IL6R	NA	-2.4794	1.950548	-9.80135	4.68E-11	1.68E-08	15.27208
CD3G	NA	-2.40335	1.921899	-6.45852	3.21E-07	1.18E-05	6.617187
BTLA	NA	-2.34143	3.352493	-5.52259	4.66E-06	9.13E-05	3.993574
KLRK1	NA	2.287793	0.820645	5.382077	6.98E-06	0.000124	3.597592
CD3D	NA	-2.27627	0.357046	-5.78658	2.18E-06	5.14E-05	4.737049
CD247	NA	-2.15903	2.257187	-8.95454	3.84E-10	8.08E-08	13.21723
IL7R	NA	-2.10977	3.068517	-6.70793	1.59E-07	7.04E-06	7.307449
SLAMF1	NA	-2.09729	3.150661	-7.09891	5.34E-08	3.26E-06	8.378287
SPP1	NA	-2.08138	-4.7399	-7.39269	2.38E-08	1.75E-06	9.172572
CLEC4M	NA	-2.01668	1.754724	-3.86386	0.000527	0.003557	-0.59763
CD209	NA	-1.94941	1.510986	-4.28334	0.000163	0.001416	0.532969
CDH1	NA	-1.92415	-2.54488	-8.77356	6.10E-10	1.10E-07	12.76512
FLT3	NA	-1.91784	2.390189	-6.3878	3.92E-07	1.36E-05	6.42057
ITK	NA	-1.90164	1.915375	-6.94077	8.29E-08	4.48E-06	7.946957
CD96	NA	-1.88345	1.194558	-9.58458	7.95E-11	2.43E-08	14.75562
CD163	NA	-1.8822	4.220506	-2.7673	0.009408	0.033809	-3.31613
GZMB	NA	-1.8792	4.353645	-6.3093	4.90E-07	1.61E-05	6.201917
ICOS	NA	-1.87882	3.183816	-6.25829	5.66E-07	1.79E-05	6.059602
TBX21	NA	-1.86153	3.871337	-4.94869	2.43E-05	0.00033	2.378655
CXCL12	NA	-1.85209	1.84454	-4.73249	4.53E-05	0.000527	1.774102
CX3CR1	NA	-1.82208	-2.28007	-5.17457	1.27E-05	0.000201	3.013214
TNFSF11	NA	-1.78881	3.349843	-4.27528	0.000167	0.001441	0.510928
CAMP	NA	1.700845	3.621482	2.565096	0.015325	0.049167	-3.76269
IL33	NA	-1.68277	4.024037	-4.17317	0.000222	0.00183	0.232799
GIMAP4	NA	-1.66951	5.156096	-5.45287	5.69E-06	0.000107	3.797097
TNFSF4	NA	1.663498	1.787824	3.741592	0.000737	0.004618	-0.92
IL1B	NA	-1.62278	1.708895	-3.39322	0.00189	0.009675	-1.8159
STAT6	NA	1.613731	1.680794	4.712592	4.79E-05	0.00055	1.718642
IL2RB	NA	-1.60221	3.06327	-5.68389	2.93E-06	6.42E-05	4.447986
S100B	NA	-1.57643	-1.30126	-3.80031	0.000627	0.004066	-0.76565
CD4	NA	-1.56424	1.814422	-10.1022	2.26E-11	1.03E-08	15.97785
CXCL2	NA	-1.54879	0.920736	-2.66656	0.012022	0.040837	-3.54124
FCGR3A	NA	-1.51058	3.22262	-2.97756	0.005569	0.022537	-2.83051
CD1D	NA	1.475974	1.519314	5.532419	4.53E-06	8.94E-05	4.021268
GAPDH	NA	1.469782	-1.27365	4.601337	6.59E-05	0.000705	1.409259
PRKCQ	NA	-1.44776	0.239816	-7.73198	9.47E-09	8.58E-07	10.07766
CTNNB1	NA	1.424278	-1.21031	7.816795	7.54E-09	7.56E-07	10.30174
IDO1	NA	-1.4106	1.977404	-3.31638	0.002317	0.011309	-2.00835
TNFRSF8	NA	-1.39602	-1.03795	-9.42691	1.17E-10	3.23E-08	14.37583
IL6	NA	-1.38437	0.095779	-3.37405	0.001989	0.010067	-1.86411
CD33	NA	-1.37604	-0.9392	-5.05433	1.79E-05	0.000261	2.675145
GATA3	NA	-1.36406	-2.21473	-7.15887	4.53E-08	2.85E-06	8.541153
IGKC	NA	-1.34716	3.602631	-2.9544	0.005904	0.023538	-2.885
SH2D1A	NA	-1.3224	1.090974	-3.83124	0.000576	0.003805	-0.684
STAT4	NA	-1.31569	1.889843	-7.81223	7.63E-09	7.62E-07	10.28971
CD40LG	NA	-1.31527	0.937201	-7.45038	2.03E-08	1.56E-06	9.327438
CCL21	NA	-1.3126	3.739173	-4.55757	7.47E-05	0.000774	1.287906
CD1A	NA	-1.30631	-0.61223	-3.94694	0.000418	0.002978	-0.37655
CCR2	NA	-1.30492	0.261207	-4.48068	9.30E-05	0.000912	1.075217
CD36	NA	-1.29668	1.975697	-2.66545	0.012054	0.040896	-3.5437
TLR10	NA	1.295199	4.131049	3.993418	0.000367	0.002694	-0.25219
CD70	NA	1.277207	0.50605	2.733822	0.010211	0.036027	-3.3915
TNFRSF13B	NA	1.275703	1.37054	5.106442	1.54E-05	0.000233	2.8216

Table S1 (*continued*)

https://dx.doi.org/10.21037/atm-22-5815

Table S1 (*continued*)

	ID	logFC	AveExpr	t	P.Value	adj.P.Val	B
MMP9	NA	-1.27468	5.897325	-3.54401	0.001262	0.007013	-1.43257
BACH2	NA	-1.27377	2.574116	-4.84936	3.24E-05	0.000406	2.100492
KLRC1	NA	-1.25373	0.29461	-4.52109	8.28E-05	0.000836	1.186903
VDR	NA	-1.24051	-0.27167	-5.9397	1.41E-06	3.65E-05	5.167443
TNFRSF11A	NA	-1.21855	-1.30586	-5.89032	1.62E-06	4.03E-05	5.028735
ANXA1	NA	-1.21091	-2.09344	-3.04394	0.004703	0.019738	-2.67308
VTCN1	NA	-1.19144	-1.69193	-15.7973	1.83E-16	8.97E-13	27.14305
FOXC2	NA	-1.17664	0.372438	-7.75464	8.91E-09	8.34E-07	10.1376
CD160	NA	-1.15743	1.22249	-5.00884	2.05E-05	0.000288	2.547412
PLCG2	NA	1.150739	3.9067	4.384808	0.000122	0.001128	0.811097
IL21R	NA	-1.1479	2.962281	-5.99521	1.20E-06	3.23E-05	5.323265
IL4	NA	-1.14545	0.170558	-6.00749	1.16E-06	3.15E-05	5.357705
TJP1	NA	-1.13645	-1.23753	-5.44306	5.86E-06	0.000109	3.769442
TBX1	NA	-1.13406	-0.62632	-4.95633	2.38E-05	0.000325	2.400096
BIRC3	NA	-1.13305	3.080678	-5.8343	1.90E-06	4.59E-05	4.871251
IRF5	NA	1.11283	2.176828	4.122411	0.000256	0.002035	0.095229
OAS1	NA	1.097464	1.528267	3.793739	0.000639	0.004123	-0.78296
GIMAP5	NA	-1.09656	4.022087	-4.33814	0.000139	0.001253	0.682979
LRRC56	NA	1.093445	0.865404	5.365731	7.32E-06	0.000129	3.551532
KIT	NA	-1.09088	-0.14316	-3.28715	0.002503	0.012002	-2.081
SELL	NA	-1.09041	3.165146	-3.9719	0.00039	0.00282	-0.30982
KLRD1	NA	-1.08849	1.169257	-5.43654	5.97E-06	0.00011	3.751062
INPP5D	NA	1.088297	3.944656	3.400601	0.001854	0.009534	-1.79731
LAT	NA	-1.07655	0.786705	-4.53767	7.90E-05	0.000808	1.232803
TLR5	NA	-1.0705	1.672048	-6.25855	5.66E-07	1.79E-05	6.060319
B2M	NA	-1.06778	2.701368	-6.22674	6.20E-07	1.93E-05	5.9715
GH1	NA	1.048282	1.453235	3.884661	0.000497	0.003412	-0.54242
TNFSF13B	NA	-1.04499	3.346657	-4.27902	0.000165	0.001429	0.521152
NCF4	NA	1.037926	2.519039	4.39403	0.000119	0.001107	0.836451
ZAP70	NA	-1.03726	0.261435	-3.27172	0.002606	0.012376	-2.11924
PPARG	NA	-1.03672	-1.66193	-3.58493	0.00113	0.006413	-1.32733
BCL11B	NA	-1.03458	-0.07582	-5.04123	1.86E-05	0.000267	2.638347
IL4R	NA	-1.03021	1.482361	-3.62299	0.001019	0.005931	-1.22901
AHR	NA	-1.02452	-0.63013	-4.49611	8.90E-05	0.000884	1.117839
CD3E	NA	-1.01623	0.719171	-8.45625	1.39E-09	2.07E-07	11.96162
BLK	NA	1.014979	4.408021	3.329321	0.00224	0.010997	-1.97608
PDCD1	NA	-1.01371	3.137734	-3.27968	0.002553	0.012168	-2.09954
PNP	NA	-1.00905	-0.84419	-4.49041	9.04E-05	0.000893	1.102105
CHD7	NA	1.002604	0.686429	6.475627	3.06E-07	1.14E-05	6.664684
PMP22	NA	-0.99542	-1.22967	-3.47702	0.001511	0.00811	-1.60377
BRCA2	NA	0.990579	0.081107	4.113416	0.000263	0.002072	0.0709
SIGLEC10	NA	0.988479	2.471812	5.397289	6.68E-06	0.000119	3.640456
CCR5	NA	-0.98833	4.984985	-2.87467	0.007212	0.02749	-3.07071
HLA-DRB1	NA	-0.98725	4.689961	-2.98943	0.005404	0.021992	-2.80251
LCP2	NA	-0.98693	1.750423	-5.69084	2.87E-06	6.36E-05	4.46757
SELP	NA	-0.98506	2.442633	-3.4544	0.001606	0.008483	-1.66126
CXCR3	NA	-0.98376	2.615984	-4.709	4.84E-05	0.000554	1.708635
IL37	NA	-0.98269	0.008787	-6.20562	6.58E-07	2.02E-05	5.912504
CD8A	NA	-0.97052	3.923451	-3.73781	0.000745	0.004649	-0.92991
C1QC	NA	-0.96211	2.227869	-2.79452	0.008799	0.032085	-3.25444
IRF9	NA	0.958441	2.309949	4.949929	2.42E-05	0.000329	2.38214
CNR2	NA	0.951777	4.760115	4.927168	2.59E-05	0.000346	2.318339
CCL18	NA	-0.94051	3.574234	-3.35838	0.002074	0.010362	-1.90341
RAB27A	NA	-0.9346	-0.54258	-3.92954	0.000439	0.003097	-0.42298
GIMAP6	NA	-0.93129	3.846123	-4.46624	9.69E-05	0.000941	1.035358
CD34	NA	-0.92618	1.711086	-4.3874	0.000121	0.001122	0.818222
C1QA	NA	-0.92356	3.843773	-4.09104	0.00028	0.002176	0.010449

Table S1 (*continued*)

https://dx.doi.org/10.21037/atm-22-5815

Table S1 (*continued*)

	ID	logFC	AveExpr	t	P.Value	adj.P.Val	B
CD14	NA	-0.9129	2.202917	-3.74757	0.000725	0.004555	-0.90433
MIF	NA	0.911591	-0.49893	3.544576	0.00126	0.007005	-1.43112
TLR7	NA	0.911146	2.754413	3.078496	0.004305	0.018438	-2.5904
FCER2	NA	-0.90633	0.992494	-4.36853	0.000128	0.001171	0.766363
ITGB1	NA	-0.90622	-1.4699	-3.56434	0.001195	0.006701	-1.38035
CD2	NA	-0.90234	6.251141	-2.67307	0.011835	0.040408	-3.52685
SLPI	NA	-0.89699	-2.37223	-2.57386	0.01501	0.048378	-3.74378
TRIM22	NA	0.885917	4.37721	4.70417	4.91E-05	0.00056	1.695182
CFI	NA	-0.87805	-2.15583	-3.39438	0.001885	0.009662	-1.81299
TFRC	NA	0.872207	-2.22034	3.280074	0.00255	0.012167	-2.09856
IL1R1	NA	-0.86491	0.260082	-4.04383	0.000319	0.002413	-0.11681
LIFR	NA	-0.86474	0.745032	-3.12225	0.003847	0.016877	-2.485
IL32	NA	-0.86228	1.229632	-4.30359	0.000154	0.001353	0.588347
RASGRP1	NA	-0.85362	1.243609	-4.63016	6.07E-05	0.000661	1.489301
TNFSF10	NA	-0.84765	2.653682	-2.95945	0.00583	0.023322	-2.87314
ACP5	NA	0.845369	3.63768	3.415095	0.001784	0.009248	-1.76075
DHX58	NA	0.844494	1.709388	3.817275	0.000599	0.003925	-0.72088
HLA-DPB1	NA	-0.84243	4.437383	-2.73515	0.010178	0.035937	-3.38852
CEACAM1	NA	0.837441	0.215366	4.285107	0.000162	0.00141	0.53779
MYD88	NA	0.829907	0.863695	4.639356	5.91E-05	0.000648	1.514847
NT5E	NA	-0.82456	-2.35972	-8.54034	1.11E-09	1.77E-07	12.17588
HLA-A	NA	0.821712	1.440567	4.914002	2.69E-05	0.000357	2.281449
FLT3LG	NA	-0.81824	1.010694	-5.55999	4.18E-06	8.42E-05	4.098962
HLA-G	NA	-0.80815	1.322908	-3.29063	0.00248	0.01191	-2.07238
CTLA4	NA	-0.80067	1.12236	-3.66027	0.000921	0.005479	-1.13229
FYN	NA	-0.79912	1.300661	-3.71636	0.00079	0.004867	-0.98606
APOBEC3G	NA	0.795667	2.51189	6.453157	3.26E-07	1.19E-05	6.602281
BTK	NA	0.790374	3.168331	4.390526	0.00012	0.001116	0.826817
IRF4	NA	0.789946	1.3818	5.221218	1.11E-05	0.000181	3.144503
CD244	NA	-0.78977	1.420861	-5.69625	2.83E-06	6.28E-05	4.482795
TNFRSF13C	NA	0.780818	3.014768	4.288055	0.000161	0.0014	0.54585
NFATC1	NA	0.776243	2.6356	3.074417	0.00435	0.018554	-2.60019
IL6ST	NA	-0.76866	0.025186	-5.06483	1.74E-05	0.000255	2.704643
TLR6	NA	0.760936	2.293283	4.163652	0.000228	0.001867	0.206977
TLR9	NA	0.757002	1.905166	3.975975	0.000386	0.002796	-0.29891
ADA	NA	-0.74742	-2.20116	-3.95125	0.000413	0.002947	-0.36504
C1QB	NA	-0.74467	4.491521	-2.88129	0.007094	0.02715	-3.0554
SAMHD1	NA	-0.74074	0.891706	-4.18724	0.000213	0.001776	0.271018
BRCA1	NA	0.734971	-1.07007	2.971891	0.005649	0.022759	-2.84388
ADRB2	NA	0.73158	2.389627	4.485458	9.17E-05	0.000903	1.088421
SOCS3	NA	-0.73112	0.65631	-3.19932	0.00315	0.014456	-2.29748
IKZF3	NA	0.729694	2.5919	4.390113	0.00012	0.001117	0.825681
CSF2	NA	-0.72908	0.023115	-5.21892	1.12E-05	0.000181	3.138038
BLNK	NA	0.718702	3.597938	3.703576	0.000818	0.005005	-1.01946
IL21	NA	-0.71315	0.542043	-3.60257	0.001077	0.006179	-1.28182
IL15	NA	-0.69718	1.793104	-2.94013	0.006121	0.024157	-2.91844
DKC1	NA	0.693543	-0.83802	4.367251	0.000128	0.001175	0.762863
SOCS1	NA	-0.68437	1.280982	-3.4288	0.001719	0.008954	-1.72611
LILRB2	NA	-0.68008	3.184239	-3.8958	0.000482	0.003335	-0.51281
DPP4	NA	-0.6703	-0.14517	-4.01527	0.000346	0.002573	-0.19356
TNFRSF1A	NA	-0.66402	-0.55851	-5.02528	1.95E-05	0.000278	2.593549
DNMT3B	NA	-0.66108	-4.79445	-3.54019	0.001275	0.007072	-1.44238
CHRNE	NA	-0.66003	0.821395	-5.68569	2.91E-06	6.41E-05	4.45305
RAG1	NA	-0.65538	-1.29307	-5.95581	1.34E-06	3.52E-05	5.212684
TNFSF13	NA	0.653941	1.504479	3.748307	0.000724	0.004549	-0.90239
PLCG1	NA	0.639548	0.076978	3.962725	0.0004	0.002878	-0.33436
RBCK1	NA	0.637127	-0.20716	5.121594	1.48E-05	0.000227	2.8642

Table S1 (*continued*)

https://dx.doi.org/10.21037/atm-22-5815

Table S1 (*continued*)

	ID	logFC	AveExpr	t	P.Value	adj.P.Val	B
NPM1	NA	0.635399	-0.49527	4.144098	0.000241	0.001943	0.153955
COMT	NA	-0.63459	-1.08445	-5.09036	1.62E-05	0.000242	2.776388
LYN	NA	0.633134	3.61532	3.922244	0.000448	0.003146	-0.44242
NCF1	NA	0.6328	4.967645	3.133197	0.003739	0.016492	-2.4585
CARD11	NA	0.631842	2.292534	2.760075	0.009576	0.034312	-3.33244
GP1BA	NA	-0.63143	2.998942	-3.37797	0.001969	0.009991	-1.85425
CD46	NA	0.624047	-0.7421	3.546193	0.001255	0.00698	-1.42697
DEF6	NA	0.619497	1.853448	4.181311	0.000217	0.001799	0.254921
TYK2	NA	0.616929	0.348497	5.636278	3.36E-06	7.17E-05	4.313892
TLR4	NA	0.616436	2.664767	3.32911	0.002241	0.011001	-1.97661
ITGB2	NA	-0.6118	2.108854	-3.69272	0.000843	0.005113	-1.0478
NCF2	NA	-0.60804	3.299559	-2.92001	0.006438	0.025187	-2.96545
IFNGR2	NA	0.607834	1.286626	7.400884	2.33E-08	1.72E-06	9.194598
FCRL3	NA	0.60699	3.668538	3.123433	0.003835	0.016846	-2.48213
KAT5	NA	0.606965	0.372061	5.764101	2.33E-06	5.39E-05	4.673788
CD59	NA	-0.60623	-0.89629	-3.88583	0.000495	0.003405	-0.53931
GP1BB	NA	-0.59991	-2.18688	-2.8757	0.007194	0.027459	-3.06832
HSPD1	NA	0.597155	-1.48124	2.748175	0.009859	0.035108	-3.35925
TNFAIP3	NA	0.594758	1.568957	3.065633	0.00445	0.01892	-2.62124
NCKAP1L	NA	0.591336	2.530371	3.878122	0.000506	0.003454	-0.55978
IRF2BP2	NA	0.590158	-0.16871	3.702083	0.000822	0.005021	-1.02336
SYK	NA	0.590153	4.274225	3.773773	0.000675	0.004302	-0.83551

https://dx.doi.org/10.21037/atm-22-5815

Table S2 The 211 differentially expressed immune-related genes between the tumor and normal samples (GSE45717)

	ID	logFC	AveExpr	t	P.Value	adj.P.Val	B
ITGB3	NA	-5.37863	9.282084	-12.1789	4.36E-09	2.42E-06	11.25423
PF4	NA	-4.54333	9.332691	-13.2757	1.35E-09	1.42E-06	12.36296
IL1B	NA	-4.43291	8.880118	-7.09975	4.02E-06	0.000153	4.527879
IL7R	NA	-4.249	8.502605	-4.87544	0.000213	0.002162	0.531446
CD36	NA	-4.16718	6.948799	-9.56859	1.04E-07	1.77E-05	8.16905
CCL5	NA	-4.03612	9.149171	-9.76752	8.01E-08	1.55E-05	8.429306
SELP	NA	-3.87931	8.479435	-9.02883	2.18E-07	2.52E-05	7.439505
SAMHD1	NA	-3.82632	9.042345	-6.94489	5.19E-06	0.000176	4.272033
ANXA1	NA	-3.73108	8.450661	-5.81137	3.69E-05	0.000639	2.295266
CLU	NA	-3.66222	8.530844	-14.151	5.64E-10	1.08E-06	13.18054
CX3CR1	NA	-3.38992	7.578126	-6.24897	1.69E-05	0.000377	3.080049
CCND1	NA	3.385463	8.716417	26.79274	6.63E-14	1.18E-09	20.70443
CD3G	NA	-3.35482	8.416163	-4.69587	0.000301	0.002801	0.181336
S100A8	NA	-3.34155	9.093329	-5.71977	4.36E-05	0.000717	2.127642
ITGA2B	NA	-3.22657	8.929751	-9.70917	8.66E-08	1.61E-05	8.353445
PTGS2	NA	-3.16521	6.811528	-5.61271	5.30E-05	0.000826	1.930259
LTF	NA	-3.02304	7.613551	-5.10624	0.000137	0.001598	0.976382
GIMAP4	NA	-2.94202	7.035267	-5.79581	3.80E-05	0.000652	2.266878
TNFSF4	NA	-2.90067	7.794499	-8.12742	8.05E-07	5.57E-05	6.140678
ITK	NA	-2.88838	7.921964	-4.32638	0.000624	0.004715	-0.54828
CCR2	NA	-2.82852	6.878606	-8.73135	3.32E-07	3.29E-05	7.022303
CD96	NA	-2.8022	7.449843	-6.064	2.35E-05	0.000477	2.751605
CD3E	NA	-2.76318	7.96063	-4.77852	0.000256	0.002488	0.342871
ITGB1	NA	-2.73255	9.618882	-8.83924	2.85E-07	3.06E-05	7.174877
S100A12	NA	-2.7249	6.989337	-5.00818	0.000165	0.001799	0.788073
LCP2	NA	-2.70212	8.399993	-6.08957	2.24E-05	0.00046	2.797305
CD3D	NA	-2.70133	7.207194	-5.04037	0.000155	0.001735	0.850017
BTLA	NA	-2.698	8.501206	-8.05301	9.00E-07	6.06E-05	6.028756
GIMAP5	NA	-2.69207	7.938385	-4.72824	0.000283	0.002669	0.244681
GP1BA	NA	-2.67157	7.777197	-8.40592	5.32E-07	4.32E-05	6.553109
AHR	NA	-2.57682	7.216585	-6.65858	8.38E-06	0.000238	3.790027
CCR4	NA	-2.55546	7.303257	-8.32496	6.00E-07	4.63E-05	6.434264
CCL3	NA	-2.53764	8.748295	-3.78164	0.001864	0.010559	-1.6387
CD4	NA	-2.53585	7.654467	-6.42942	1.24E-05	0.000306	3.395781
CD14	NA	-2.51747	8.712835	-4.10963	0.000962	0.006429	-0.98074
BMP6	NA	-2.50688	8.154067	-10.2145	4.49E-08	1.07E-05	8.997901
CLEC12A	NA	-2.50003	6.202993	-5.0362	0.000156	0.001747	0.841986
PRKCQ	NA	-2.49565	7.296953	-5.6023	5.40E-05	0.000836	1.910986
CD2	NA	-2.4599	7.132974	-4.94656	0.000185	0.00195	0.669173
NT5E	NA	-2.40497	6.38169	-5.9013	3.14E-05	0.000573	2.458732
ITGB2	NA	-2.34266	9.436504	-7.08522	4.12E-06	0.000154	4.504006
HBA1	NA	-2.29516	9.073168	-6.53698	1.03E-05	0.000269	3.581762
CLEC7A	NA	-2.19935	6.450692	-4.20005	0.000802	0.005612	-0.80002
CD86	NA	-2.15934	7.156517	-8.63911	3.79E-07	3.47E-05	6.890694
CCL3L1	NA	-2.11832	9.104742	-3.3984	0.004062	0.018901	-2.4073
FLT3	NA	-2.11233	6.342857	-6.17395	1.93E-05	0.000413	2.947432
RNASE3	NA	-2.08258	6.888763	-5.73555	4.23E-05	0.000702	2.156601
GZMB	NA	-2.0757	7.8351	-5.87563	3.29E-05	0.000587	2.412191
ITGAX	NA	-2.07544	8.022211	-7.61724	1.76E-06	9.10E-05	5.358229
CD28	NA	-2.05421	6.928059	-4.48494	0.000456	0.003757	-0.23383
LAT	NA	-2.03298	8.414415	-6.73873	7.32E-06	0.000217	3.926146
PTX3	NA	-1.98255	6.018638	-3.53198	0.003095	0.015427	-2.13992
ICOSLG	NA	1.979555	8.621774	7.438971	2.33E-06	0.000108	5.076418
SH2D1A	NA	-1.94979	6.862683	-4.35578	0.000588	0.004519	-0.48984
SERPINA1	NA	-1.92485	7.629112	-3.53752	0.003061	0.015303	-2.12883
S100A9	NA	-1.92423	8.190146	-4.10897	0.000963	0.006433	-0.98208
CLEC4E	NA	-1.91313	5.351123	-3.08341	0.007705	0.030934	-3.03254

Table S2 (*continued*)

https://dx.doi.org/10.21037/atm-22-5815

Table S2 (*continued*)

	ID	logFC	AveExpr	t	P.Value	adj.P.Val	B
MMP8	NA	-1.90459	5.111232	-4.04692	0.001091	0.007057	-1.1063
SELL	NA	-1.88485	10.06285	-4.14451	0.000897	0.006095	-0.91098
SLAMF6	NA	-1.86912	8.830733	-4.90687	0.0002	0.002064	0.592388
RASGRP1	NA	-1.8472	8.340094	-5.30391	9.40E-05	0.001222	1.352524
LCN2	NA	-1.84473	7.622743	-6.53726	1.03E-05	0.000269	3.582244
CD40LG	NA	-1.79776	5.554132	-5.47834	6.79E-05	0.000968	1.680379
ICOS	NA	-1.7787	5.936771	-4.05473	0.001074	0.00697	-1.09067
CCL20	NA	-1.76714	5.694856	-3.38273	0.004194	0.019352	-2.4386
DPP4	NA	-1.76714	5.994984	-4.05815	0.001067	0.006937	-1.08382
IL1RN	NA	-1.75618	6.362322	-3.88062	0.001526	0.009042	-1.43992
KLRD1	NA	-1.74808	6.187355	-3.66221	0.002375	0.012638	-1.8786
SLAMF1	NA	-1.74006	6.539589	-7.03534	4.47E-06	0.000162	4.421877
NLRP3	NA	-1.73482	7.721816	-3.06459	0.008004	0.031789	-3.06955
NCF2	NA	-1.72569	8.456846	-3.74993	0.001988	0.011048	-1.70242
IRAK3	NA	-1.7138	7.035374	-2.92191	0.01068	0.039619	-3.34856
TREM1	NA	-1.70261	6.658125	-3.7132	0.002142	0.011727	-1.7762
GIMAP6	NA	-1.65279	7.515436	-4.43993	0.000498	0.004002	-0.3229
TNFSF10	NA	-1.64713	7.308011	-8.81704	2.94E-07	3.10E-05	7.143604
IL32	NA	-1.63275	8.203102	-4.378	0.000563	0.004378	-0.44571
IL4R	NA	-1.59746	9.598201	-5.14806	0.000126	0.001502	1.056345
TLR8	NA	-1.59624	6.294023	-4.37062	0.000571	0.004427	-0.46035
IL6ST	NA	-1.58958	8.578379	-3.31702	0.004794	0.021454	-2.56967
ARPC1B	NA	-1.58672	10.44459	-9.99753	5.93E-08	1.29E-05	8.724643
CCR1	NA	-1.57827	6.637221	-4.97716	0.000175	0.001875	0.728278
MPL	NA	-1.57569	7.403507	-6.36176	1.39E-05	0.00033	3.277934
TNF	NA	-1.57293	7.526785	-2.78176	0.014154	0.049174	-3.61925
TYROBP	NA	-1.56344	8.818782	-4.70668	0.000295	0.002765	0.202498
PIK3CA	NA	1.546402	8.969081	6.581673	9.54E-06	0.000255	3.658555
LEPR	NA	-1.52806	7.152895	-5.6974	4.54E-05	0.000736	2.086524
TNFSF13B	NA	-1.52087	6.867676	-6.82748	6.31E-06	0.000198	4.075787
EIF2AK2	NA	1.515311	8.096611	5.431879	7.40E-05	0.001028	1.593435
CD163	NA	-1.5135	6.305524	-4.17903	0.000837	0.005798	-0.842
IL6R	NA	-1.50555	7.760218	-6.70063	7.80E-06	0.000229	3.861562
PRF1	NA	-1.50305	8.539865	-3.06773	0.007954	0.031651	-3.06339
CD33	NA	-1.50169	7.25594	-5.90603	3.11E-05	0.000571	2.467306
CSF3R	NA	-1.47402	7.603482	-3.79902	0.0018	0.010297	-1.6038
CD244	NA	-1.43246	6.94105	-4.52224	0.000423	0.003584	-0.16012
FHL1	NA	-1.4267	7.816043	-4.44131	0.000497	0.004001	-0.32016
CD69	NA	1.418387	10.49255	4.496482	0.000445	0.003711	-0.21101
CD247	NA	-1.4004	7.42604	-4.38534	0.000555	0.004343	-0.43114
IL18	NA	-1.39147	4.543753	-4.94845	0.000185	0.001945	0.67284
CFP	NA	-1.32741	7.621652	-4.96215	0.00018	0.00191	0.6993
ICAM2	NA	-1.32045	8.89803	-7.16752	3.60E-06	0.000143	4.638758
MAPK8	NA	1.315296	8.65948	7.362504	2.63E-06	0.000117	4.954177
IL2RB	NA	-1.3085	7.507569	-3.93161	0.001376	0.008374	-1.33754
BCL11B	NA	-1.28746	7.865818	-3.69084	0.002241	0.012115	-1.8211
MEFV	NA	-1.26178	7.311186	-4.30545	0.00065	0.00484	-0.58992
TGFB1	NA	-1.24846	9.504369	-5.37691	8.20E-05	0.0011	1.490208
CXCL2	NA	-1.23011	6.506754	-3.14235	0.006837	0.028207	-2.91631
CLEC4D	NA	-1.21259	5.385323	-2.94285	0.010238	0.038356	-3.30781
BCL2L1	NA	-1.21122	8.559229	-5.05795	0.00015	0.001695	0.88378
MAPK14	NA	-1.19622	8.031008	-9.08068	2.03E-07	2.52E-05	7.511098
TLR10	NA	-1.18319	8.48787	-3.10957	0.007307	0.029673	-2.981
CYCS	NA	1.171775	9.062436	5.585735	5.57E-05	0.00085	1.880293
ITGAL	NA	-1.16613	9.126593	-4.61318	0.000354	0.003155	0.019041
GAPDH	NA	-1.16111	11.47616	-6.61936	8.95E-06	0.000248	3.723092
TGFBR1	NA	1.160826	9.061441	9.783223	7.85E-08	1.54E-05	8.449662

Table S2 (*continued*)

https://dx.doi.org/10.21037/atm-22-5815

Table S2 (*continued*)

	ID	logFC	AveExpr	t	P.Value	adj.P.Val	B
CASP1	NA	-1.14989	8.561087	-4.30337	0.000653	0.004852	-0.59405
LYST	NA	-1.13961	8.787217	-4.75473	0.000269	0.002566	0.296439
IL12A	NA	1.139438	6.581383	4.011327	0.001172	0.007426	-1.17764
CD8A	NA	-1.13183	7.824094	-3.63353	0.002518	0.013188	-1.93619
PSMB9	NA	-1.12374	9.770962	-6.81569	6.43E-06	0.0002	4.055979
TNFRSF13C	NA	1.118974	9.568466	4.604012	0.00036	0.003199	0.001017
NLRP12	NA	-1.11405	6.557306	-3.85129	0.001619	0.009464	-1.4988
TNFRSF1B	NA	-1.10266	8.636796	-3.92089	0.001406	0.008511	-1.35906
IL1A	NA	-1.08698	4.939777	-3.59986	0.002696	0.013946	-2.00378
IRF4	NA	1.073555	8.885989	4.273535	0.000693	0.005049	-0.65347
CXCR5	NA	1.069492	8.405519	3.080183	0.007755	0.031063	-3.03888
JUN	NA	1.063351	9.383574	2.975199	0.009591	0.036467	-3.24472
STAT5B	NA	-1.06053	8.665859	-8.0379	9.21E-07	6.08E-05	6.005928
RHD	NA	-1.06008	6.32956	-3.67283	0.002325	0.012449	-1.85729
NLRC4	NA	-1.06006	5.877551	-3.52258	0.003155	0.015639	-2.15877
U2AF1	NA	1.053571	8.600477	5.92226	3.02E-05	0.00056	2.496672
NOD2	NA	-1.0413	6.729926	-5.20923	0.000112	0.001386	1.172941
FAS	NA	-1.04048	7.18275	-7.79719	1.33E-06	7.70E-05	5.638266
STXBP2	NA	-1.02858	9.039753	-5.76589	4.01E-05	0.00068	2.21218
PYCARD	NA	-1.02256	7.90997	-6.20969	1.81E-05	0.000394	3.010707
TNFRSF1A	NA	-1.01803	7.468659	-4.49901	0.000443	0.003698	-0.20602
ADAM17	NA	0.994027	9.017996	5.945519	2.90E-05	0.00055	2.538698
P2RX7	NA	-0.98528	7.073159	-4.3246	0.000626	0.004726	-0.55182
CD300LF	NA	-0.98518	6.967653	-3.98428	0.001238	0.007717	-1.23187
REL	NA	0.981528	10.10981	3.5198	0.003173	0.015701	-2.16434
CORO1A	NA	-0.97808	10.61024	-6.19808	1.85E-05	0.000401	2.990179
IKBKE	NA	-0.9773	7.853331	-8.84669	2.82E-07	3.06E-05	7.185369
SPN	NA	-0.97476	8.024771	-3.77904	0.001874	0.01059	-1.64393
CXCR4	NA	0.971547	11.84997	7.493145	2.14E-06	0.000101	5.162526
CXCR3	NA	-0.96781	7.038224	-6.40853	1.28E-05	0.000314	3.359473
UNC13D	NA	-0.96752	8.096089	-7.86786	1.19E-06	7.17E-05	5.747024
RAC2	NA	-0.96029	9.718136	-4.06788	0.001046	0.006829	-1.06432
IL17RA	NA	-0.95491	8.60198	-5.18284	0.000118	0.00143	1.122703
PRKCD	NA	-0.93259	9.194209	-3.5272	0.003125	0.015527	-2.1495
DKC1	NA	0.924868	8.389842	4.892243	0.000206	0.002107	0.564034
CD274	NA	0.924374	5.406502	4.632154	0.000341	0.003074	0.05634
IKZF1	NA	-0.9227	9.665849	-4.8931	0.000205	0.002106	0.565688
ITGA4	NA	-0.91598	9.499474	-4.00554	0.001186	0.007497	-1.18924
SLC11A1	NA	-0.91573	7.597137	-3.18038	0.006329	0.026476	-2.84111
VDR	NA	-0.91389	6.48895	-4.41267	0.000526	0.004175	-0.37691
TFRC	NA	0.903827	9.118023	3.223724	0.005795	0.024816	-2.75519
CIITA	NA	-0.90006	9.882884	-4.06864	0.001044	0.006825	-1.0628
LILRB2	NA	-0.89767	8.009604	-3.53939	0.003049	0.015257	-2.12506
HLA-DPB1	NA	-0.89263	11.35136	-6.1894	1.88E-05	0.000405	2.974795
HAVCR2	NA	-0.8916	6.33564	-3.17036	0.006459	0.026884	-2.86093
HLA-E	NA	-0.88235	11.74065	-7.12533	3.86E-06	0.00015	4.569807
TLR5	NA	-0.88043	6.488195	-4.29983	0.000658	0.004872	-0.60111
TNFRSF17	NA	-0.87403	5.726458	-2.94932	0.010105	0.037978	-3.2952
CD70	NA	0.873658	7.5497	3.533456	0.003086	0.015399	-2.13697
CD55	NA	0.867373	9.832008	5.857237	3.40E-05	0.0006	2.378784
ADA	NA	-0.8651	7.532385	-5.58546	5.57E-05	0.00085	1.879776
BRCA2	NA	0.86313	5.54983	3.562984	0.002906	0.014728	-2.07775
NRAS	NA	0.856522	9.616677	7.072746	4.20E-06	0.000156	4.483505
JAK3	NA	-0.85485	8.678183	-5.90294	3.13E-05	0.000573	2.46171
RAB27A	NA	-0.85437	8.000761	-4.46539	0.000474	0.003854	-0.27249
ITGAM	NA	-0.85256	7.573397	-3.64884	0.002441	0.012867	-1.90544
VWF	NA	-0.85233	6.556426	-4.86509	0.000217	0.002194	0.511358

Table S2 (*continued*)

https://dx.doi.org/10.21037/atm-22-5815

Table S2 (*continued*)

	ID	logFC	AveExpr	t	P.Value	adj.P.Val	B
LILRB1	NA	-0.8509	8.211945	-2.8986	0.011193	0.040954	-3.39383
TGFB2	NA	-0.83917	6.21494	-3.8972	0.001475	0.008809	-1.40662
FCGR1A	NA	-0.83335	5.221652	-2.95372	0.010016	0.037725	-3.28662
WDR1	NA	-0.82592	10.68916	-5.41984	7.57E-05	0.001044	1.570854
GATA2	NA	-0.82453	7.284386	-5.0498	0.000152	0.001717	0.868129
CASP3	NA	0.794223	7.841942	3.271859	0.005255	0.023022	-2.65957
HP	NA	-0.78615	5.371592	-3.03865	0.008436	0.033176	-3.1205
KRAS	NA	0.781433	8.55993	4.649912	0.000329	0.002985	0.091213
IL15	NA	-0.78012	5.676656	-3.02191	0.008727	0.034021	-3.15334
CCR7	NA	0.766675	10.62601	4.699049	0.000299	0.002791	0.187553
TPI1	NA	-0.75783	8.684928	-7.09185	4.07E-06	0.000153	4.514895
LTBR	NA	-0.75168	7.091528	-3.78847	0.001838	0.010443	-1.62498
CHUK	NA	0.747385	7.743892	4.385896	0.000554	0.00434	-0.43003
XIAP	NA	0.742263	7.364187	3.918203	0.001414	0.00854	-1.36445
RELB	NA	0.716497	8.30302	2.87535	0.01173	0.042472	-3.43889
ALOX5	NA	0.708848	10.03028	3.366691	0.004333	0.019822	-2.47062
COMT	NA	-0.69536	8.476	-5.18715	0.000117	0.001427	1.130903
TNFSF9	NA	0.692365	7.833685	2.847883	0.012396	0.044289	-3.492
GATA3	NA	-0.68424	7.062541	-3.4114	0.003956	0.018539	-2.38133
MYO5A	NA	0.681197	8.625516	2.809432	0.013391	0.047034	-3.56611
VAV1	NA	-0.67739	8.535164	-3.91479	0.001424	0.008578	-1.37131
IL27RA	NA	-0.67457	8.143211	-5.315	9.21E-05	0.001201	1.373471
ELF4	NA	-0.65875	7.996843	-4.73028	0.000282	0.002661	0.248669
NFE2L2	NA	0.650126	8.530494	3.557677	0.002938	0.014846	-2.0884
HFE	NA	-0.64649	5.873079	-5.64672	4.98E-05	0.00079	1.993124
STAT2	NA	-0.63759	9.41475	-3.53951	0.003048	0.015257	-2.12483
IL10RB	NA	-0.63743	9.049835	-5.58148	5.61E-05	0.000853	1.872395
BIRC2	NA	0.63084	8.861359	4.069731	0.001042	0.006815	-1.06062
CREBBP	NA	0.630745	9.687881	5.900812	3.14E-05	0.000573	2.457851
LYN	NA	0.629063	10.92456	3.526258	0.003131	0.015548	-2.15139
HLA-DPA1	NA	-0.62906	12.06943	-3.63566	0.002507	0.013141	-1.93192
IL10RA	NA	0.621421	10.38763	3.535988	0.00307	0.015336	-2.13189
PTPN2	NA	0.618951	8.269377	3.548386	0.002994	0.015065	-2.10703
MDM2	NA	0.617463	8.298324	4.930219	0.000191	0.001998	0.637582
CARD11	NA	0.609514	8.671536	5.018925	0.000161	0.001778	0.80876
IL2RG	NA	-0.60798	10.0719	-3.71566	0.002131	0.011679	-1.77125
DNASE1	NA	-0.6052	6.879174	-3.07984	0.007761	0.031071	-3.03957
CXCL1	NA	-0.59804	7.006248	-3.71102	0.002151	0.011763	-1.78058
CCR3	NA	-0.5951	5.066051	-3.78524	0.001851	0.010494	-1.63149
DHCR24	NA	-0.59421	6.704014	-5.04897	0.000152	0.001719	0.866541

https://dx.doi.org/10.21037/atm-22-5815

Table S3 The average rankings of 77 common differentially expressed immune-related genes via 10-fold cross-validation using a SVM-RFE algorithm

FeatureName	FeatureID	AvgRank
GATA3	34	3.2
CD247	14	5.9
CD28	15	7.5
IL6R	47	9.6
CD4	21	9.7
HLA-DPB1	40	10.6
CD3E	19	11.6
ICOS	41	12.7
TLR10	70	14
ITK	53	14.1
LYN	58	14.7
GZMB	39	15.1
CD96	25	15.2
NT5E	60	15.6
IRF4	50	15.9
GIMAP4	35	17.2
IL7R	49	19.4
PRKCQ	61	19.6
CD3G	20	20.3
CCND1	8	20.4
BCL11B	4	21.6
CD3D	18	23.5
LCP2	56	23.8
CD40LG	22	24.2
BTLA	6	24.3
TLR5	71	25.7
FLT3	32	26
VDR	77	26.1
IL4R	46	27.8
GIMAP6	37	28.5
GAPDH	33	29
GIMAP5	36	29.8
CXCR3	29	33.3
CD8A	24	34.2
SLAMF1	68	34.6
TNFRSF13C	72	35.2
ITGB1	51	35.6
ADA	1	38.6
CD70	23	38.6
SELP	66	42.1
TNFSF10	74	42.1
LILRB2	57	43.5
CD244	13	45.1
IL2RB	44	46.4
SELL	65	47
DKC1	30	48.1
ITGB2	52	48.8
TNFSF4	76	51.2
COMT	26	51.3
TFRC	69	52.6
CD33	16	52.7
LAT	55	53.1
SH2D1A	67	53.8
IL6ST	48	54.3
CD14	10	54.9
CD163	11	55.1
SAMHD1	64	55.5
RAB27A	62	56.2
CXCL2	28	56.4
GP1BA	38	57.2
BRCA2	5	58.6
CD2	12	60.4
CD36	17	60.4
DPP4	31	61
KLRD1	54	61.3
IL1B	43	63.9
ANXA1	3	64.6
CX3CR1	27	64.6
IL15	42	64.7
AHR	2	65.2
CCR2	9	66.4
TNFSF13B	75	67.7
NCF2	59	68
IL32	45	68.1
RASGRP1	63	68.7
TNFRSF1A	73	69.3
CARD11	7	70

Table S3 (*continued*)

Table S3 (*continued*)

https://dx.doi.org/10.21037/atm-22-5815

Table S4 The 26 immune-related hub genes selected using a random forest algorithm

	normal	tumor	MeanDecreaseAccuracy	MeanDecreaseGini
CD96	0.080333	0.037016	0.048578089	0.941935484
ITK	0.06	0.009079	0.015666667	0.727741935
CD4	0.053333	0.014667	0.022820513	0.686451613
LCP2	0.052	0.017	0.022545455	0.660645161
GIMAP6	0.026667	0.008444	0.012820513	0.658064516
ICOS	0.046667	0.006167	0.01034965	0.632258065
IL6R	0.045	0.007175	0.011414141	0.632258065
IRF4	0.02	0.001818	0.003333333	0.624516129
GIMAP5	0.01	0.002222	0.003636364	0.500645161
PRKCQ	0.02	0.0025	0.004444444	0.454193548
CD40LG	0.02	0.006667	0.01	0.40516129
CD3D	0.016667	0.007778	0.010598291	0.361290323
GATA3	0.03	0.008889	0.013426573	0.332903226
IL2RB	0.032	0.013571	0.018	0.32516129
SH2D1A	0.01	0.002	0.003333333	0.283870968
CD28	0.013333	0.003077	0.005	0.270967742
CD3E	0.02	0.002	0.003636364	0.270967742
CD3G	0.02	0.002	0.003636364	0.255483871
GIMAP4	0	0	0	0.255483871
LAT	0.01	0.001667	0.002857143	0.255483871
BRCA2	0	0	0	0.237419355
FLT3	0.02	0.0025	0.004444444	0.216774194
LILRB2	-0.005	-0.002	-0.002857143	0.216774194
TLR5	0.006667	0.002857	0.004	0.193548387
CD247	0.013333	0.004444	0.006666667	0.167741935
GZMB	0.01	0.004	0.005714286	0.139354839

https://dx.doi.org/10.21037/atm-22-5815

Table S5 The 63 familiar immune checkpoint molecules and the 41 immune checkpoint molecules in GSE93291

63 familiar immune checkpoint molecules	41 immune checkpoint molecules in GSE93291
CD80	BTLA
CD86	BTN1A1
CD273	BTN2A1
CD274	BTN2A2
CD275	BTN3A1
CD276	BTN3A2
VTCN1	BTN3A3
VSIR	BTNL2
NCR3LG1	BTNL3
HHLA2	BTNL8
CD28	BTNL9
CTLA-4	CD200
CD279	CD200R1
ICOS	CD27
TMIGD2	CD274
BTLA	CD276
HVEM	CD28
TNFSF14	CD40
BTN1A1	CD80
BTN2A1	CD86
BTN2A2	CEACAM1
BTN2A3	HAVCR1
BTN3A1	HHLA2
BTN3A2	ICOS
BTN3A3	IDO1
BTNL2	IL2RB
BTNL3	KIR3DL1
BTNL8	LAG3
BTNL9	LAIR1
BTNL10	NCR3LG1
SKINTL	PVR
TNFRSF9	SIGLEC10
TNFSF9	SIGLEC15
CD27	SIGLEC9
CD70	TIGIT
CD40	TMIGD2
TNFSF5	TNFRSF18
TNFRSF18	TNFRSF9
TNFSF18	TNFSF14
TNFRSF4	TNFSF18
TNFSF4	VTCN1
TNFRSF25	
IDO1	
LAG3	
GAL3	
TIGIT	
CD266	
PVR	
PVRL2	
TIM3	
CEACAM1	
HAVCR1	
SIGLEC15	
SIGLEC9	
SIGLEC10	
CD200R1	
CD200	
LAIR1	
ADORA2A	
KIR3DL1	
SLAM	
NAIL	
IL2RB	

https://dx.doi.org/10.21037/atm-22-5815

Table S6 The 65 differentially expressed genes of the MCL molecular clusters in GSE93291

	ID	logFC	AveExpr	t	P.Value	adj.P.Val	B
IGKV1OR2-108	NA	1.725786	9.891089	4.054258	8.81E-05	0.003222	1.217952
GATA3	NA	1.661045	7.52284	10.99958	4.58E-20	9.96E-16	34.22037
CD3E	NA	1.533081	9.340488	10.7921	1.47E-19	1.60E-15	33.13177
ICOS	NA	1.487337	8.011179	7.710273	3.49E-12	6.34E-09	17.17792
UBASH3A	NA	1.441929	7.469967	6.787777	4.17E-10	3.63E-07	12.67496
MIRLET7DHG	NA	-1.39599	5.436358	-4.21669	4.73E-05	0.002156	1.789733
ITK	NA	1.335994	10.16584	9.610046	1.10E-16	5.98E-13	26.93171
CHRM3-AS2	NA	1.319179	6.640439	5.327256	4.52E-07	0.000107	6.112613
DAPK1-IT1	NA	1.317312	6.349707	5.035428	1.64E-06	0.000252	4.911914
LOC541472	NA	1.313824	6.945098	5.336134	4.34E-07	0.000106	6.149803
LOC101928173	NA	1.302212	6.525837	5.222522	7.21E-07	0.000144	5.676812
LGALS2	NA	1.257316	8.376114	4.676772	7.48E-06	0.00063	3.497142
HIST1H3B	NA	-1.25651	5.971813	-3.28853	0.00131	0.016778	-1.23821
LOC100130744	NA	1.251725	6.474463	3.550655	0.000544	0.009955	-0.44373
CLEC4G	NA	1.247639	6.332951	3.91782	0.000147	0.004456	0.750852
RGL4	NA	1.241336	6.171024	4.886389	3.10E-06	0.000368	4.315552
FCAMR	NA	1.233756	8.882764	3.692392	0.000331	0.007358	0.006382
CD7	NA	1.221377	7.669667	7.528463	9.12E-12	1.32E-08	16.274
DBH-AS1	NA	1.214772	7.165114	5.482219	2.25E-07	6.69E-05	6.767061
C1QA	NA	1.202467	9.971415	5.222496	7.21E-07	0.000144	5.676706
IGFBP4	NA	1.188228	9.155561	4.942455	2.44E-06	0.000321	4.538513
IGKV1OR2-118	NA	1.178275	10.34301	4.157538	5.95E-05	0.002518	1.579568
CCL21	NA	1.177312	11.88468	4.33749	2.95E-05	0.001618	2.225716
LAMP3	NA	1.166764	9.032171	7.186134	5.44E-11	7.39E-08	14.59271
HIST1H2AE	NA	-1.1628	6.172081	-3.59067	0.000473	0.009158	-0.3181
ITGB2-AS1	NA	1.158801	9.352488	8.450758	6.55E-14	1.53E-10	20.92418
GIMAP4	NA	1.153945	9.577252	7.661143	4.53E-12	7.04E-09	16.93296
IL32	NA	1.146985	10.6535	6.741181	5.27E-10	4.25E-07	12.45365
XXYLT1	NA	-1.14056	6.37961	-3.71177	0.000309	0.00709	0.069002
CD5L	NA	1.139343	5.876073	3.306695	0.001235	0.016182	-1.18479
LAT	NA	1.138842	9.24213	10.0969	7.25E-18	5.26E-14	29.48214
CLEC4M	NA	1.136007	6.899561	3.870316	0.000175	0.004892	0.591112
LRRC52	NA	1.134241	6.635244	4.28439	3.64E-05	0.001818	2.03296
KCNMA1-AS1	NA	1.122273	6.284585	4.650462	8.34E-06	0.000663	3.39615
TBC1D4	NA	1.120043	9.594577	8.907928	5.37E-15	1.67E-11	23.2777
BLID	NA	1.11623	5.561732	4.994848	1.95E-06	0.000277	4.748377
IGK	NA	1.112652	10.7369	4.396901	2.33E-05	0.001364	2.443421
ERV9-1	NA	-1.09491	5.297691	-4.58342	1.10E-05	0.000802	3.140603
RGS13	NA	1.092277	5.061149	3.161243	0.001974	0.021485	-1.60572
SCGB3A1	NA	1.083837	4.880187	3.917169	0.000147	0.00446	0.748653
FAM111B	NA	-1.07981	6.465732	-4.04109	9.26E-05	0.003315	1.172354
RPS11	NA	-1.073	8.64878	-3.33126	0.001139	0.01544	-1.11214
FAM30A	NA	1.066288	5.935028	4.800437	4.46E-06	0.000469	3.977037
KLK1	NA	1.063356	7.788423	5.011356	1.81E-06	0.000266	4.814797
AICDA	NA	1.061618	5.207496	2.855943	0.005031	0.038443	-2.43656
DEFB114	NA	-1.0616	3.251285	-3.25746	0.00145	0.017799	-1.32905
CTSW	NA	1.056524	7.723959	4.140112	6.36E-05	0.002605	1.518076
LOC100652768	NA	1.051942	7.529488	4.141099	6.34E-05	0.002602	1.521555
PRKCQ	NA	1.046411	8.241333	9.044692	2.53E-15	1.02E-11	23.98628
P2RY13	NA	1.042396	8.417228	5.521527	1.88E-07	5.92E-05	6.934844
BTNL8	NA	1.040863	5.397862	3.698448	0.000324	0.007282	0.02593
LOC200772	NA	1.036349	6.757967	3.464044	0.000731	0.011894	-0.71177
LOC101930452	NA	-1.0361	4.885293	-3.48843	0.000673	0.011332	-0.63686
IFI44L	NA	1.029892	9.596683	2.902035	0.004388	0.035093	-2.3158
C1QC	NA	1.025014	10.27267	4.954184	2.32E-06	0.000312	4.585366
TRAC	NA	1.024629	11.68657	7.677973	4.15E-12	6.94E-09	17.01681
PTK2B	NA	1.022714	8.781337	4.145533	6.23E-05	0.002586	1.537187
CD3D	NA	1.021117	11.69704	6.008716	1.92E-08	9.31E-06	9.070514
SOCS2-AS1	NA	1.019459	5.417911	4.207945	4.90E-05	0.002202	1.758527
NOG	NA	1.019158	4.891756	3.392039	0.000931	0.013734	-0.93048
CNDP1	NA	1.010564	4.857911	3.989375	0.000112	0.003735	0.9943
LINC00943	NA	1.006716	5.813805	4.383566	2.46E-05	0.001411	2.394369
LRRC25	NA	1.006531	8.02439	3.792852	0.000231	0.005825	0.333879
BTBD11	NA	1.006402	6.026008	5.937572	2.70E-08	1.18E-05	8.752451
TNIK	NA	1.002548	6.650659	8.003599	7.32E-13	1.45E-09	18.65045

https://dx.doi.org/10.21037/atm-22-5815

Table S7 The 20 prognostic differentially expressed genes of the MCL molecular clusters in GSE93291

	coef	se	z	p	HR	HRse	HRz	HRp	HRCILL	HRCIUL
FCAMR	-0.774	0.231	-3.354	0.001	0.461	0.106	-5.064	0	0.315	0.674
LGALS2	-0.716	0.23	-3.116	0.002	0.489	0.112	-4.553	0	0.335	0.713
ICOS	-0.703	0.233	-3.013	0.003	0.495	0.116	-4.371	0	0.337	0.727
CD3D	-0.664	0.23	-2.89	0.004	0.515	0.118	-4.101	0	0.353	0.751
GATA3	-0.66	0.228	-2.892	0.004	0.517	0.118	-4.096	0	0.355	0.752
PRKCQ	-0.649	0.231	-2.808	0.005	0.522	0.121	-3.954	0	0.357	0.764
UBASH3A	-0.645	0.228	-2.828	0.005	0.525	0.12	-3.971	0	0.361	0.764
BTBD11	-0.61	0.231	-2.636	0.008	0.543	0.126	-3.632	0	0.371	0.795
LAMP3	-0.555	0.231	-2.402	0.016	0.574	0.133	-3.21	0.001	0.393	0.84
HIST1H2AE	-0.572	0.239	-2.388	0.017	0.565	0.135	-3.222	0.001	0.381	0.837
FAM30A	-0.544	0.234	-2.321	0.02	0.58	0.136	-3.085	0.002	0.395	0.853
ITK	-0.533	0.23	-2.318	0.02	0.587	0.135	-3.063	0.002	0.402	0.856
IGFBP4	0.521	0.229	2.275	0.023	1.684	0.386	1.773	0.076	1.155	2.454
IGKV1OR2-108	-0.525	0.23	-2.279	0.023	0.592	0.136	-2.997	0.003	0.405	0.864
ERV9-1	0.524	0.239	2.19	0.029	1.689	0.404	1.704	0.088	1.139	2.504
IGKV1OR2-118	-0.48	0.229	-2.097	0.036	0.619	0.142	-2.691	0.007	0.425	0.902
C1QA	0.485	0.234	2.076	0.038	1.625	0.38	1.645	0.1	1.106	2.387
RPS11	-0.486	0.234	-2.076	0.038	0.615	0.144	-2.673	0.008	0.419	0.904
P2RY13	-0.471	0.229	-2.051	0.04	0.625	0.143	-2.619	0.009	0.428	0.911
LRRC52	-0.459	0.228	-2.016	0.044	0.632	0.144	-2.559	0.011	0.434	0.919

https://dx.doi.org/10.21037/atm-22-5815

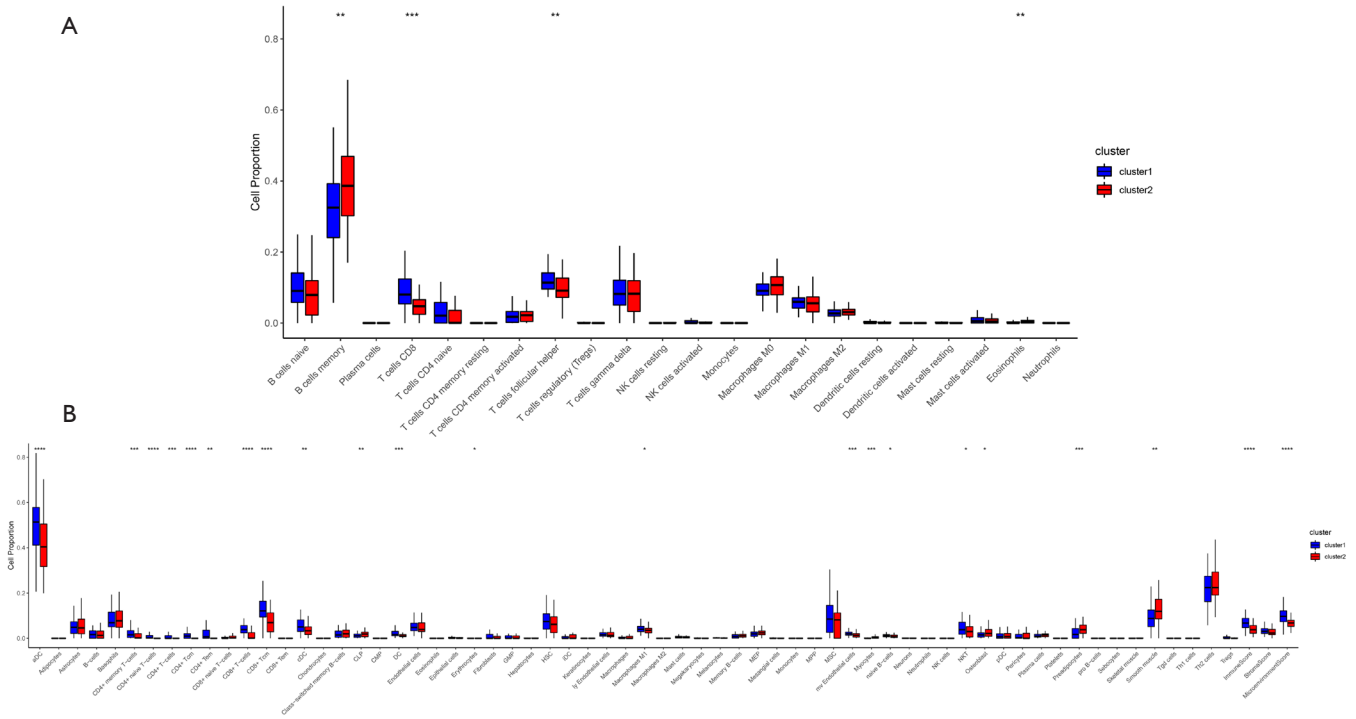

Figure S1 The immune cell infiltration proportion in the MCL molecular clusters (GSE93291). The immune cell infiltration proportion in the TME of the two clusters was analyzed by CIBERSORT and xCell, respectively. ****, P<0.0001; ***, P<0.001; **, P<0.01; *, P<0.05. TME, tumor microenvironment; MCL, mantle cell lymphoma.

https://dx.doi.org/10.21037/atm-22-5815